

SHAPE MEMORY ALLOY ACTUATOR CONTROL FOR 3D STEERING OF  
ACTIVE SURGICAL NEEDLE IN MINIMAL INVASIVE SURGERIES

A DISSERTATION SUBMITTED TO THE GRADUATE DIVISION OF THE  
UNIVERSITY OF HAWAI'I AT MANOA IN PARTIAL FULFILLMENT  
OF THE REQUIREMENTS FOR THE DEGREE OF  
DOCTOR OF PHILOSOPHY  
IN  
MECHANICAL ENGINEERING

APRIL 2020

By

Saeed Karimi

Dissertation Committee:

Bardia Konh, Chairperson

Peter Berkelman

Mohammad Elahinia

Mehrdad Ghasemi Nejjhad

Scott Miller

Aaron Ohta

## **Acknowledgements**

I would like to thank many people at University of Hawaii at Manoa who helped and supported me. I would like to specially thank my Ph.D. advisor Dr. Bardia Konh, and my Thesis Committee Members, Dr. Mehrdad Ghasemi Nejhada, Dr. Scott Miller, Dr. Mohammad Elahinia, Dr. Peter Berkelman, and Dr. Aaron Ohta for all their helps and supports. I would also like to thank my family and loved ones. This work was financially supported by Hawaii Community Foundation, Grant ID # 18ADVC-90805, that I am grateful for.

## **Abstract**

Minimally Invasive Surgery (MIS) is defined as a surgical procedure that is associated with lower postoperative patient's morbidity, compared to the conventional approach for the same diagnostic/therapeutic operation. Minimally invasive percutaneous interventional procedures for diagnostics and therapeutics are practiced in a variety of medical procedures such as brachytherapy, biopsy, and thermal ablation. The clinical outcome in such procedures is subjected to precise navigation and accurate placement of the needle at specific target locations within the soft tissue. Active needle steering increases the target placement accuracy, and consequently improves the clinical outcome. In this work, a 3D steerable active flexible needle with multiple interacting Shape Memory Alloy (SMA)-wire actuators is introduced. A self-sensing resistive-based feedback loop control system was designed and implemented to control the SMA's actuation. The needle tip position was controlled through the feedback loop control system using the electrical resistance measurements of the SMA-wire actuators. Concomitant actuation and sensing capabilities of SMAs were used in the control system to realize a desired 3D motion at the needle tip. The controller was then tested on a 1:4 scaled prototype of the active needle for reference path tracking. This work demonstrates the 3D steerable active needle manipulation via precision control of interacting SMA-wire actuators.

# Table of Contents

Acknowledgements .....	i
Abstract .....	ii
List of Figures .....	v
List of Tables.....	viii
List of Symbols .....	ix
List of Abbreviations.....	x
Chapter 1 Introduction .....	1
Chapter 2 Theoretical Background .....	9
2.1. SMA Actuators.....	9
2.2. SMA Constitutive Models.....	12
2.3. SMA Control .....	18
Chapter 3 Research Methods and Materials.....	22
3.1. 3D Steerable Active Surgical Needle .....	22
3.2. Experimental Setup .....	24
3.3. Kinematics of the Active Flexible Needle .....	26
3.3.1. Three-axis coordinate system.....	26
3.3.2. Translation of the SMA-wire Actuators' Strain to Needle Displacement.....	30
3.4. SMA Self-Sensing Electrical Resistance Feedback Control .....	32
3.5. Tracking System.....	34
Chapter 4 Results and Discussions.....	35
4.1. Characterization of the 3D Steerable Active Needle with Multiple Interacting SMA-wire Actuators .....	35
4.1.1. Characterization of the Active Flexible Needle Response to Actuation .....	36
4.1.2. SMA-wire Actuator Characterization .....	45
4.2. SMA Self-Sensing Electrical Resistance Feedback Control .....	51

4.2.1. Tracking Control of a Single SMA-wire Actuator .....	51
4.4.2. Tracking Control of the 3D Steerable Active Needle via Control of Multiple Interacting SMA-Wire Actuators .....	55
Chapter 5 Conclusion .....	57
References .....	59
List of Publications.....	70
Appendix .....	77
A1. Control Algorithm Flowchart .....	77

## List of Figures

<b>Figure 2.1.</b> Critical stress-temperature profiles used in Brinson model [24] .....	15
<b>Figure 2.2.</b> schematic illustration of shape memory alloys control concept: model-based feed-forward control, feedback control (PID), linearized plant concept and strain-resistance model position sensing (smart actuator concept) [20] .....	21
<b>Figure 3.1.</b> Schematic of the 3D steerable active needle structure; A: soft joint, B: rigid link, C: three SMA-wire actuators passed and looped through the needle internal structure, D: interior tube, E: rigid needle base ( $D_{out}=6\text{mm}$ , $D_{in}=1.5\text{mm}$ ) .....	24
<b>Figure 3.2.</b> Schematic view of the experimental setup (left), active needle prototype with three SMA-wire actuators (right). The 40g of mass applies a total prestress of 5.55 MPa, on each SMA-wire actuator.....	26
<b>Figure 3.3.</b> Kinematic model concept of the active needle with three SMA-wire actuators. The three actuators independently induce a deflection along their corresponding actuation axis $\chi_i$ . Top view of the active needle is shown.....	27
<b>Figure 3.4.</b> Schematic illustration of the deformation of the flexible joints during the actuation of SMA-wire actuators.....	31
<b>Figure 3.5.</b> Kinematics characteristics of the active flexible active needle; 3DoF RR-configured manipulator.....	31
<b>Figure 3.6.</b> Control system architecture: multi-actuation and self-sensing electric resistance feedback control of multiple SMA-wire actuators.....	33

<b>Figure 4.1.</b> Electric current: SMA-wire actuation signal in characterization experiments.....	36
<b>Figure 4.2.</b> Deflected shape of the active needle prototype under single SMA-wire actuation in direction of each SMA actuator.....	38
<b>Figure 4.3.</b> Position tracking (3D displacement measurement) of the active needle tip under single actuation duty cycles for the three SMA-wire actuators; ACTR1, ACTR2, and ACTR3.....	39
<b>Figure 4.4.</b> Position tracking (3D displacement measurement) of the active needle tip under dual actuation duty cycles; parallel actuation of pair sets of the three SMA-wire actuators; {ACTR1, ACTR2}, {ACTR1, ACTR3}, and {ACTR2, ACTR3} .....	40
<b>Figure 4.5.</b> Travel path of the active needle; position of the needle at the tip in XY-coordinates (Cartesian coordinate system) under single and dual actuation duties.....	42
<b>Figure 4.6.</b> 3D spatial workspace of the active needle; multi-actuation of the SMA-wire actuators in parallel enables manipulation of the active needle to place the tip at target points within 20mm radial distance on XY-plane.....	44
<b>Figure 4.7.</b> SMA-wire actuator self-sensing characteristic; A. electric resistance vs. electric power, and mapping the active needle response to SMA-wire characteristics. The data was obtained with three repetitions on the wires (note small error bars); B. needle deflection vs. electric power, C. needle deflection vs. electric resistance, for ACTR1.....	48

**Figure 4.8.** SMA-wire actuator self-sensing characteristic; A. electric resistance vs. electric power, and mapping the active needle response to SMA-wire characteristics. The data was obtained with three repetitions on the wires (note small error bars); B. needle deflection vs. electric power, C. needle deflection vs. electric resistance, for ACTR2.....49

**Figure 4.9.** SMA-wire actuator self-sensing characteristic; A. electric resistance vs. electric power, and mapping the active needle response to SMA-wire characteristics. The data was obtained with three repetitions on the wires (note small error bars); B. needle deflection vs. electric power, C. needle deflection vs. electric resistance, for ACTR3.....50

**Figure 4.10.** SMA-wire actuator self-sensing characteristic: A. electric resistance vs. power, and mapping the response characteristics of the SMA-wire; The data was obtained with three repetitions on the wires (note small error bars); B. deflection (actuation strain) vs. electric power, C. deflection (actuation strain) vs. electric resistance for single SMA- wire actuator under tension.....52

**Figure 4.11.** Control system performance in position tracking of a single SMA-wire actuator: tracking reference and response of the SMA-wire (top) and tracking error (bottom).....54

**Figure 4.12.** Reference tracking control (position control) of the active needle at the tip, under multi-actuation duties; controlled actuation of the actuators ACTR1, and ACTR2, for a reference path following task; following the straight vertical line path (yellow line) .....56



## List of Tables

<b>Table 3.1.</b> Kinematic model concept of the active needle: system's response to multi-actuation schemes, change-of-coordinate matrices converting between the Cartesian and the three-axis skew coordinates dividing the XY-plane into three 13 plane zones.....	29
---	----

## List of Symbols

A	area
C	specific heat
D	diameter
ER	electrical resistance
$I_H$	high amplitude electric current
$I_L$	low amplitude electric current
h	convection heat transfer coefficient
I	electric current
m	mass
P	power
$R_d$	desired resistance
T	temperature
$T_D$	time delay
$\xi$	martensite volume fraction
$\rho$	electrical resistivity
$\rho_m$	electrical resistivity of martensite
$\rho_a$	electrical resistivity of austenite

## **List of Abbreviations**

CV	Coefficient of Variations
MIS	Minimally Invasive Surgeries
PE	Pseudo-elasticity
PW	Pulse Width
PWM	Pulse Width Modulation
PWPF	Pulse Width Pulse Frequency
SD	Standard Deviation
SMA	Shape Memory Alloy

# **Chapter 1**

## **Introduction**

In recent decade, the increased tendency towards the concept of Minimally Invasive Surgery (MIS), due to its reduced tissue trauma, shortened recovery time, and decreased postoperative complications, has prompted a demand for new surgical tools to be applied in precise navigation through the tissue towards the target locations [1], in order to expand the applications of MIS. Navigating medical devices are applied in a variety of diagnostic and therapeutic treatments such as laparoscopy, endoscopy, colonoscopy, and suturing. However, the practical application of such medical instruments is constrained by various complexities ranging from fundamental procedure issues, e.g., limited space, to the issues related to surgical tools, such as lack of dexterity in manipulation, lack of actuation force, and low visualization quality.

Hypodermic needles, and cannulas are a category of such navigating surgical instruments that require precise manipulation at their tip [2]–[4]. Minimally invasive needle-based percutaneous procedures are increasingly practiced in medical diagnosis and

interventions, over the past decade. For instance, needle insertion is a current technique practiced for cancer interventions in several medical procedures such as brachytherapy, biopsy, and thermal ablation [5]. Although, such minimally invasive surgical procedures offer significant benefits, but also give rise to several major challenges since the targeting accuracy is limited due to the anatomical obstacles in the needle's path, movements in the target position caused by tissue deformation, and undesired bending of the needle during insertion [4]. Current surgical needles can only provide limited control on the trajectory between entry point and the target in soft tissue [6]. Probable targeting error can affect the diagnosis and therapeutic outcome.

Minimally Invasive Surgery (MIS) is defined as a surgical procedure that is associated with lower postoperative patient's morbidity, compared to the conventional approach for the same diagnostic/therapeutic operation [7]. MIS has evolved along minimizing the invasiveness of the surgical procedures, in view of the recent technological advancements in instrumentation and enhancement of dexterity, by means of robotic systems [8]–[13]. MIS minimizes the trauma to the tissue through minimizing the size and the number of surgical incisions, subsequently resulting in a reduced patient's recovery time [12]. This has prompted an increasing demand for MIS over the past two decades [14].

Minimally invasive percutaneous interventional procedures such as biopsy [15], and brachytherapy [16], have attracted interest in recent years. Percutaneous needle insertion

techniques are practiced in a variety of medical procedures for diagnostics and therapeutics such as blood sampling [17], regional anesthesia [18], neurosurgery [19], and thermal ablation [20]. The clinical outcome in such procedures is subjected to precise navigation and accurate placement of the needle at specific target locations within the soft tissue. However, the targeting accuracy is limited due to movements of the target caused by deformation of the soft tissue, undesired deflections of the needle during the insertion [21], and imaging inaccuracies. The requisite tolerance for the accuracy of needle insertion in clinical practices varies by the application. For instance, in kidney, liver, and breast biopsies, and in prostate brachytherapy, a placement accuracy of millimetres is required, while in brain, eye, and ear, a placement accuracy of micro-millimetre is demanded [22]. However, significant errors are common in current clinical practices, mainly due to the tissue deformations [23]. A case study on the accuracy of the needle placement for implanting radioactive seeds in prostate brachytherapy, practiced on 20 patients by an experienced clinician, pointed an average placement error of 6.3 *mm* [24], which is a sizeable error compared to the size of a normal prostate gland, 38 × 25 × 32 *mm* (transverse diameter × sagittal diameter × height) [25]. Inserting needle into soft tissue exerts forces on the tissue; deforming the tissue, and displacing the target locations [26].

Active needle steering capacitates the clinicians to compensate the targeting errors, and increase the needle placement accuracy in percutaneous interventions; consequently, improves the clinical outcome [21]. Active steerable needle can track complex trajectories,

and steer around anatomical obstacles and critical organs to access the target locations within the soft tissue while minimizing the targeting errors, and maintaining the benefits of MIS compared to open surgery [27], [28]. A control system based on the steering model of the active needle can reject the disturbances arising from the tissue deformation, deflection of the needle during insertion, and inaccurate insertion angle.

In this work, the kinematics and dynamics of a 3D steerable active surgical needle [13] (designed in AMMI Lab) are studied. The novel design of the needle; the multi-link flexible structure with multiple interacting Shape Memory Alloy (SMA) wire actuators, enhances the steerability of the needle. The kinematic analysis, and dynamical modeling of the needle is essential for active control application in percutaneous needle insertions.

Passive needles steer in the tissue via lateral translation and choice of rotation at their proximal end (i.e., the needle base). The passive bevel-tip needles are manipulated by rotating the needle around its shaft while pushing the needle forward toward the target point. The passive needle steering depends on the geometry of the bevel tip (e.g. bevel angles) and mechanism of needle–tissue interactions. In addition, their control functionality is restricted by limited availability of sensory feedback.

Compared to passive needles, active flexible needles can potentially reach the targets with more accuracy via an appropriate actuation and control [29]. Another clinical advantage of the active needles is capacitating the clinicians to correct any possible misalignments in needle insertion, without tangling with complications of the needle–tissue interactions. An appropriate control system can modify inaccuracies in the needle insertion angle and reject the disturbances due to bending of the needle and tissue deformation to compensate for the targeting errors [30]. An active needle can track complex trajectories in percutaneous interventions, while maintaining benefits of minimally invasive surgery (MIS) compared to open surgery. The active needle steering reduces the number of needle insertions in clinical procedures and hence minimizes the tissue trauma to patients and thereby expedites the patients' recovery [31], [32].

Movement of target due to breathing, organ movement, needle bending, poor needle visualization, and limited imaging possibilities were listed among challenges in needle-based interventions [33]. It was reported [33] that a mean maximal error of 2.7mm in needle placement is acceptable in targeting lesions in needle-based interventions. Recognizing the importance of precision tracking and placement, several efforts have been made in recent years to improve medical imaging and interventional delivery systems, but without addressing the needle design. The design of most clinical needles is several decades old. Also, with conventional rigid needles, only a straight path towards the target is feasible. However, in many needle insertion procedures, it is desired to curve the needle towards the target to



avoid anatomical obstacle(s) [33]. Several needle steering techniques [2], [3], [34]–[37] have been suggested to guide the needle inside the tissue. The steering techniques [38], [39] can be grouped into four categories: (i) tissue manipulation, (ii) lateral needle manipulation, (iii) tip-based steering, and (iv) “shaft-based” steering. Passive needles have been proposed in the past decade for diagnosis or therapeutic purposes. Bevel-tip [40], pre-curved [41], [42], kinked needles, flexure-based needles [43], and concentric pre-curved tubes [44], [45] are among the most effective needle steering methods. However, trajectory planning with passive needles is complicated and sometimes inaccurate [46], [47].

A major challenge in needle-based interventional procedures is to conform to the shape of an organ, mainly due to the needle’s geometry and lack of proper actuation [48].

In recent studies [49]–[53], an active steerable needle was introduced with a considerable planar deflection in tissue. The design demonstrates a potential capacity in steering and target placement with an improved accuracy within the soft tissue, by means of smart actuators. For instance, the active needle introduced by Active Needle Technology Ltd [54] reduces penetration force and thus tip deflection and provides better visualization via longitudinal ultrasonic vibrations. Several needle manipulation techniques have also been proposed in CoBra project, similar to the works found in [2].

Shape Memory Alloys (SMAs) are a unique class of smart materials with the ability to recover their deformed shapes, caused by a loading condition, through temperature changes resulting in a high actuation energy density [55]. This unique characteristic pertains to reversible crystalline phase transition between *austenitic* high temperature phase and two *martensitic* low temperature phases, i.e., *twinned*, and *detwinned*. These phases differ in their crystal structure, and transition between the phases is a diffusionless transformation, occurring by shear lattice distortion [56].

Remarkable characteristics of SMAs, i.e., Shape Memory Effect (SME) and Pseudoelasticity (PE) [55], along with the material properties such as high corrosion resistance [57], bio-compatibility [58], and non-magnetic [59] have made SMAs appropriate alternatives for applications in biomedical domain [60] including orthopaedics [61], orthodontics [62], cardiology [63] and surgical instruments [64]. A notable advantage of using SMAs as actuators in medical devices is that their actuation can be related to their electrical resistance [65]. SMAs can be used as actuators and positioning sensors via precise control [66] and measurements of the electrical resistance under functional duties.

This research work introduces a steerable active surgical needle that can steer around the anatomical obstacles and critical organs to access the targets within the soft tissue and improve the targeting accuracy by use of smart actuators [21]. Additionally, an active smart needle can track complex trajectories in percutaneous interventions, while maintaining

benefits of MIS compared to open surgery [1]. A control system based on steering model of the needle can reject potential disturbances from bending of the needle during insertion, inaccurate insertion angle, and tissue deformation, subsequently compensate for the targeting error [4].

The aims and objectives of this research study are to investigate design analysis and control of SMA actuators in applications of active steerable surgical devices. For this purpose, and to accurately predict the actuator's output in active surgical tools, studying the characteristics of SMAs and the phase transformation process in SMAs during the actuation (duty cycles) is a crucial step. This research aims to test and verify the feasibility of SMA actuation in active surgical needles and measure the actuation performance of an active surgical needle prototype to realize a controlled 3D manipulation. Obtaining a consistent and reliable actuation remains a challenge in design and development of SMA-activated systems due to SMA's nonlinear behavior and large hysteresis [67]. This work is aiming to design a control system with an efficient algorithm for controlling the motion of SMA active devices.

## Chapter 2

### Theoretical Background

#### 2.1. SMA Actuators

*Sensors* execute sensing by converting a mechanical signal into a non-mechanical output (e.g., voltage), while *actuators* convert a non-mechanical input (e.g., electrical power) into a mechanical output. *Active materials* are a type of multifunctional materials that exhibit sensing and actuation capabilities. Active actuators exhibit a mechanical response when subjected to a non-mechanical field (thermal, electrical, magnetic, etc.). Strain recovery in SMAs, is caused by the phase transformation between the two martensite and austenite phases during the changes in the temperature under loading conditions. The phase transformation i.e., shape recovery, occurs even under high loads, hence SMAs hold a high actuation energy density. The forward transformation, in which the austenite phase transforms to the martensite phase, initiates at *martensite start temperature*,  $M_s$  and completes at *martensite finish temperature*,  $M_f$ . Similarly, the reverse transformation, in which the martensite phase transforms to the austenite phase, initiates at *austenite start temperature*,  $A_s$  and completes at *austenite finish temperature*,  $A_f$  [68]. The phase-transformation temperatures are generally

determined under stress-free conditions. SMAs, however, exhibit low frequency response and large hysteresis [55], [69].

In active control of SMAs, the shape recovery is implemented thermally by *electrical* heating, or *inductive* heating. However, the electrical heating (*Joule heating*) is more common in controlling SMA actuators, since the inductive heating causes uneven heating of the actuator, which results in a microstructural stress in the material.

A privileged advantage of SMAs as actuators is their self-sensing capabilities. Along with the strain recovery, the electrical resistance of an SMA actuator alters notably during the transformation [66]. This phenomenon can be applied to develop a feedback positioning control using the electrical resistance variations to measure strain. Due to a correlation between the actuation and the electrical resistance [65], SMAs are well suited for use as smart actuators [69]. This postulates a concomitant use of SMAs as actuators and positioning sensors with precise control, and measurement of the electrical resistance under functional duties [66], [70]. The electrical resistance of an SMA wire actuator changes during the actuation cycle due to the changes in geometry. The relation between the electrical resistance variations and the strain during transformation is determined quantitatively [65], [71].

In Joule heating method, the electric current drives and heats up the SMA actuator. The electrical power,  $P_{electric}$ , delivered to the actuator is:

$$P_{electric} = I^2 R \quad (\text{Eq. 2.1})$$

where  $I$  is the electrical current and  $R$  is the electrical resistance of the shape memory alloy actuator.

The thermodynamic equation governing the energy equilibrium during the martensitic transformation is:

$$mC \frac{dT(t)}{dt} + m\Delta H \frac{d\xi(t)}{dt} = hA(T_\infty - T(t)) + I^2 R \quad (\text{Eq. 2.2})$$

where  $C$  is the specific heat of the alloy,  $m$  and  $A$  are the mass and external area of the actuator,  $h$  is the convection heat transfer coefficient,  $\Delta H$  is the latent heat for the transformation,  $\xi$  is the fraction concentration of martensite in the alloy, and  $T_\infty$  is the ambient temperature.

Tracking changes in electrical properties of SMAs during martensitic transformation, allows monitoring the martensitic transformation, and consequently the state of the actuator. Moreover, SMA's function as a sensor is defined by its ability to track the shape by monitoring the changes in electrical properties.

In shape memory alloys, the electrical resistivity in martensite phase is higher than austenite phase. SMA's resistivity in state of phase transformation, i.e., at temperatures that both martensite and austenite phases coexist, is estimated as fraction concentration of each phase:

$$\rho = \xi\rho_m + (1 - \xi)\rho_a \quad (\text{Eq. 2.3})$$

where  $\rho_m$  and  $\rho_a$ , are the electrical resistivity of martensite and austenite phases, respectively and  $\xi$  is the fraction concentration of martensite in the alloy.

The relationship between the martensitic fraction concentration and deformation is linear. The relationship between the actuator displacement and electrical resistance, under a constant load, is approximately linear, although hysteretic. It is important to note that the relationship between electrical resistance and strain is also a function of mechanical load [66], [72]. To use an SMA actuator as a sensor, and correspondingly control SMA actuators, a model for the resistance–strain relationship is required [71].

## **2.2. SMA Constitutive Models**

The physical behavior of SMA is a function of three relevant variables: stress, strain and temperature. Several different constitutive models are developed to predict the behavior of SMA materials as a function of these variables. Three major constitutive models of SMA

materials used to study the static performance of SMAs attributed to *Tanaka, Liang and Rogers*, and *Brinson* [73].

One of the primary constitutive models of SMAs is developed by Tanaka [74]. Tanaka model assumes a unified one-dimensional (1D) martensitic phase transformation. The model suggests the strain, temperature, and martensite volume fraction, are the only state variables, and the stress is determined by those variables. The phase transformation kinetics is also described as a function of stress and temperature. Yet, this is limited only to the stress-induced martensite phase transformation. Liang and Rogers [75] proposed a model based on the rate form of the Tanaka constitutive model [76]. Tanaka, and Liang and Rogers models can both explain the direct phase transformations from martensite to austenite and the reverse transformation from austenite to martensite; however, they are unable to explain the detwinning process of martensite [76]. Their model doesn't capture the SME behavior at lower temperatures, which is a cause of conversion between the stress-induced martensite and the temperature-induced martensite. This major drawback for both Tanaka, and Liang and Rogers models has been resolved in Brinson model [68]. Brinson model defines the total martensite volume fraction as a summation of two terms; the stress-induced, and the temperature-induced martensitic volume fractions.

The constitutive equation of Brinson model describes the state variables stress ( $\sigma$ ), strain ( $\varepsilon$ ), and temperature ( $T$ ) in the terms of the martensite volume fraction ( $\xi$ ). In Brinson



model, the martensite volume fraction ( $\xi$ ) is the sum of stress-induced ( $\xi_S$ ) and temperature-induced components ( $\xi_T$ ):

$$\xi = \xi_S + \xi_T \quad (\text{Eq. 2.4})$$

The original form of the constitutive equation is as follows [68]:

$$\sigma - \sigma_0 = E(\xi)\varepsilon - E(\xi_0)\varepsilon_0 + \Omega(\xi)\xi_S - \Omega(\xi_0)\xi_{S0} + \Theta(T - T_0) \quad (\text{Eq. 2.5})$$

where  $(\sigma_0, \varepsilon_0, \xi_0, T_0)$  signify the initial state of the material. The modulus of elasticity,  $E$ , is assumed as a linear function of the martensite volume fraction:

$$E(\xi) = E_A + \xi(E_M - E_A) \quad (\text{Eq. 2.6})$$

$\Theta$  is the thermoelastic coefficient.  $\Omega$  is the phase transformation coefficient, defined as:

$$\Omega(\xi) = -\varepsilon_L E(\xi) \quad (\text{Eq. 2.7})$$

where,  $\varepsilon_L$  is the maximum recoverable strain.

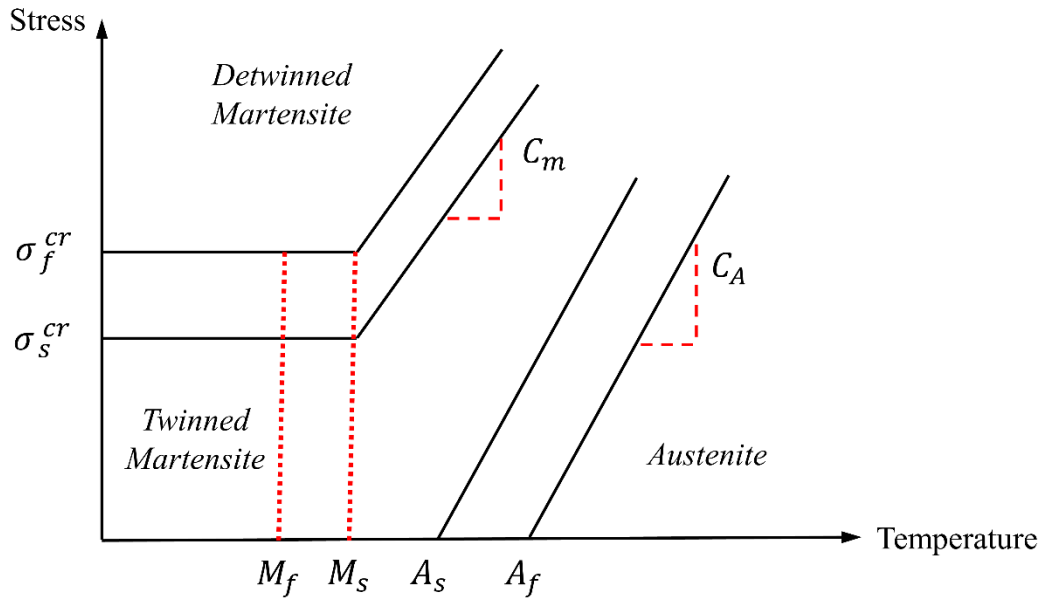


**Figure 2.1.** Critical stress-temperature profiles used in Brinson model [73].

Figure 2.1 presents the critical stress-temperature profile used in Brinson constitutive model.  $C_A$  and  $C_M$  are two material constants called stress-influence coefficients, which indicate the impact of stress on the transition transformation and are usually determined experimentally.

The evolution kinetics equations to calculate the martensite fractions as a function of temperature and stress, according to Figure 2.1, are defined as:

- *Conversion to detwinned martensite*

For  $T > M_S$  &  $\sigma_S^{cr} + C_M(T - M_S) < \sigma < \sigma_f^{cr} + C_M(T - M_S)$

$$\xi_S = \frac{1 - \xi_{S0}}{2} \cos \left\{ \frac{\pi}{\sigma_S^{cr} - \sigma_f^{cr}} [\sigma - \sigma_f^{cr} - C_M(T - M_S)] \right\} + \frac{1 + \xi_{S0}}{2} \quad (\text{Eq. 2.8})$$

$$\xi_T = \xi_{T0} - \frac{\xi_{T0}}{1 - \xi_{S0}} (\xi_S - \xi_{S0})$$

For  $T < M_S$  &  $\sigma_S^{cr} < \sigma < \sigma_f^{cr}$

$$\xi_S = \frac{1 - \xi_{S0}}{2} \cos \left\{ \frac{\pi}{\sigma_S^{cr} - \sigma_f^{cr}} [\sigma - \sigma_f^{cr}] \right\} + \frac{1 + \xi_{S0}}{2} \quad (\text{Eq. 2.9a})$$

$$\xi_T = \xi_{T0} - \frac{\xi_{T0}}{1 - \xi_{S0}} (\xi_S - \xi_{S0}) + \Delta_{T\varepsilon}$$

where, if  $M_f < T < M_S$  &  $T < T_0$

$$\Delta_{T\varepsilon} = \frac{1 - \xi_{T0}}{2} \{ \cos[a_M(T - M_f)] + 1 \}$$

*else*

$$\Delta_{T\varepsilon} = 0$$

- *Conversion to austenite*

*For  $T > A_S$  &  $C_A(T - A_f) < \sigma < C_A(T - A_S)$*

$$\xi = \frac{\xi_{S0}}{2} \left\{ \cos \left[ a_A \left( T - A_S - \frac{\sigma}{C_A} \right) \right] + 1 \right\} \quad (2.10)$$

$$\xi_S = \xi_{S0} - \frac{\xi_{S0}}{\xi_0} (\xi_0 - \xi)$$

$$\xi_T = \xi_{T0} - \frac{\xi_{T0}}{\xi_0} (\xi_0 - \xi)$$

where  $a_A$ ,  $a_M$ ,  $b_A$  and  $b_M$  are material constants, in terms of transition temperatures  $A_S$ ,  $A_f$ ,  $M_S$  and  $M_f$ . The above-mentioned equations describe direct and reverse

phase transformations in SMAs in the form of nonlinear functions. It should be noted that these equations follow different loading and unloading paths on the phase transformation diagram, describing the hysteresis behavior of the material.

Different 3D constitutive models have also been developed for SMA materials by *Boyd and Lagoudas* [77], *Ivshin and Pence* [78], and *Graesser and Cozzarelli* [79]. However, these 3D constitutive models are complex to solve and require a large number of parameters to be defined. Brinson model has been chosen for this work for its ability to accurately predict the 1D actuation of SMAs, and its applicability to our experiments with 1D SMA wires.

### **2.3. SMA Control**

Precise control of SMA actuators is challenging due to their highly non-linear behavior, large hysteresis, low bandwidth, slow response, and saturation of the shape memory effect [69], [80]. To control the position of SMA actuators, two general types of control schemes have been researched; model-based feedforward control, and feedback loop control. In model-based feedforward control process, a reverse dynamic model of the SMA actuator, is exploited in the control system to compensate the hysteresis effect [65], [79], [81]–[84]. On the other hand, the function of feedback control loop is to improve and stabilize the actuation performance of the SMA actuator, taking up the position, temperature, or electrical

resistance of the SMA actuator as the state variable in the feedback signal of the control system [65], [85]–[87].

Therewith, number of control systems for controlling SMA actuators have been proposed in the literature. SMA control approaches are classified as [80]: **i. linear control systems**; classical PID controllers [88], and Pulse Width (PW) modulated PD, PI, and PID controllers [89], **ii. Pulse Width Modulation (PWM) based control systems**; Pulse Width Pulse Frequency (PWPF) modulation [90], and time division PWM network [91], **iii. Sensor-less control systems**; feedforward [92] and feedback [93] controlled, internal electrical resistance feedback with neural networks [65], and **iv. nonlinear control systems**; variable structure control [94], segmented binary control [95], segmented discrete state control [96], time delay control [97], force tracking control [98], and sliding mode control [99].

The general concept of the control strategies that can be implemented on SMA actuators is illustrated in Figure 2.2. The solid black line path corresponds to classic PID control with external position sensor. The linearizing concept is sketched by the dashed line path, and the positive feedback scheme is used to linearize the actuator plant, hence, the controller is fronted to a linearized plant. The grey path implements a feed-forward control scheme based on the current-strain model of the actuator, when activated. Lastly, in the smart

actuator concept, the dotted line path, based on the resistance-strain model of the actuator estimates the position [69].

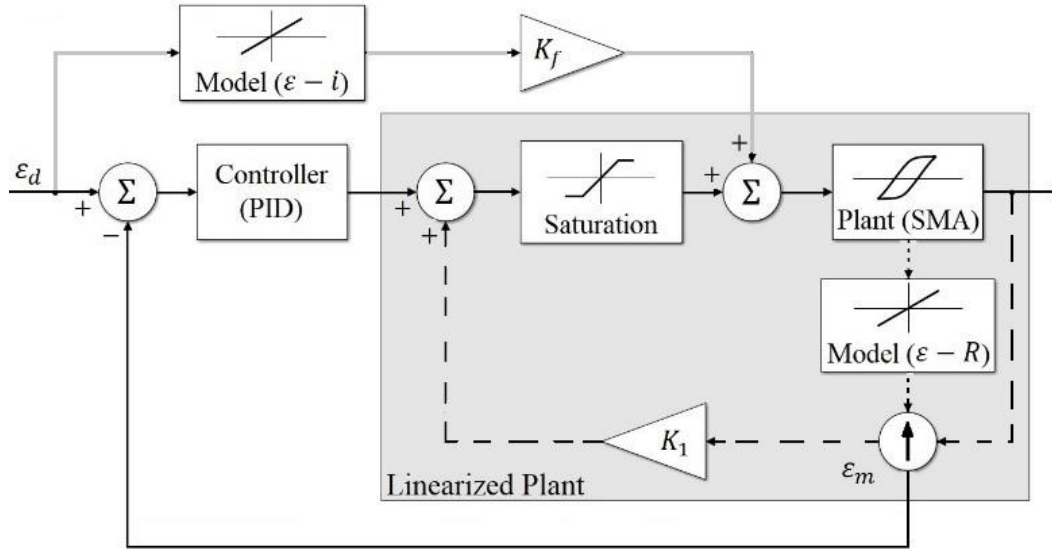


**Figure 2.2.** schematic illustration of shape memory alloys control concept: model-based feed-forward control, feedback control (PID), linearized plant concept and strain-resistance model position sensing (smart actuator concept) [20].

The smart actuation i.e., combination of sensing and driving functions on the same component, is the proposed control scheme in this work. The resistance–strain model of an SMA actuator is used to estimate the position of a shape memory actuator, where the resistance of the actuator is directly computed by measuring the voltage and the electric current. An accurate estimation of the displacement (strain) of the actuator is achievable if the resistance-strain model of the actuator is properly defined, and thus the actuator can also

be used as a sensor. Thus, a closed loop control system is implementable using the position estimation feedback.



## Chapter 3

### Research Methods and Materials

#### 3.1. 3D Steerable Active Surgical Needle

To validate and measure the feasibility and precision of the self-sensing control for trajectory tracking task, tests have been performed on a prototype (designed at AMMI Lab) of an SMA-actuated active flexible needle. The prototype is a 1:4 scaled model of 17-gauge hypodermic needle ( $D_o=6\text{mm}$ ,  $D_i=1.5\text{mm}$ ) comprised of 3D printed parts; rigid base and links, and soft joints (prototyped by ©PROTOLABS, Inc.). Figure 3.1 illustrates the designed model of the active needle. This new configuration is designed to achieve 3D steering and increased steerability. The purpose of employing soft joints in this design configuration is to enhance the flexibility. The needle is actuated by three SMA-wire (NiTi) actuators to realize a 3D displacement. Nitinol (NiTi) alloys are made of 55%-56% Nickel and 44%-45% Titanium. The three pairs of equiangularly distanced holes embedded on each of the link and joint components allows for the three SMA-wire actuators to pass and loop through needle internal structure. The triangular alignment hole in the center is designed to facilitate concentric alignment of the NiTi wire actuators by means of an alignment rod. The soft joint

pieces are fabricated with ©PROTOLABS' Digital Clear/Translucent Photopolymer material at Shore A hardness 60, with the tensile strength of 4.5 MPa, and 170% elongation at break. The needle base and links are fabricated with Somos® PerForm polymeric material which

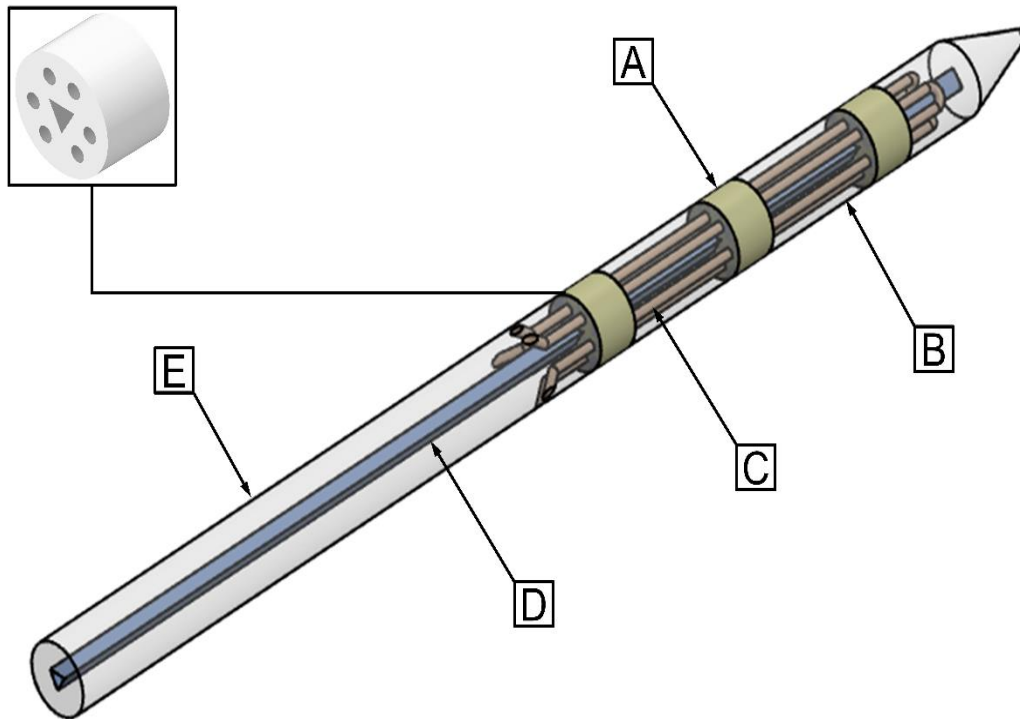


**Figure 3.1.** Schematic of the 3D steerable active needle structure; **A:** soft joint, **B:** rigid link, **C:** three SMA-wire actuators passed and looped through the needle internal structure, **D:** interior tube, **E:** rigid needle base ( $D_{out} = 6\text{mm}$ ,  $D_{in} = 1.5\text{mm}$ ,  $L = 80\text{mm}$ ).  $D_{out}$  and  $D_{in}$  are the outer and inner diameter of the tube, respectively, and  $L$  is the total length. has a tensile strength of 68 MPa, and heat deflection temperature (HDT) of 132°C and 82°C at the stress levels of 0.46 MPa and 1.81 MPa, respectively.

### 3.2. Experimental Setup

The experimental setup used for testing the active needle prototype is illustrated in Figure 3.2. Three SMA-wire actuators were connected to a triple output programmable DC power supply (RIGOL DP832, RIGOL Technologies), and actuated via *Joule* heating. In all experiments, the SMA-wire actuators were equally pretensioned by 40g of mass attached to the bottom ends of the wires, shown in Figure 3.2. The 40g of mass applies a total prestress of 5.55MPa on each SMA-wire actuator. The SMA-wire actuators were trained with 80 cycles of heating and cooling prior to the experiment. The training results in a more consistent cyclic response of SMAs [100], which is beneficial for control system with multiple actuation duties. The power supply is equipped with a built-in output (voltage, and electric current) sensing module that measures the voltage, and electrical current across the SMA wires with  $10mV/1mA$  measurement resolution, during actuation duty cycles. The position at the needle tip was tracked via a vision tracking program in MATLAB<sup>®</sup>. The images were captured using a Canon PowerShot SX60 HS with a 3.8-247.0mm 1:3.4-6.5 USM lens at 1280×720 30fps, during the actuation.

Understanding the loading path of each actuator on the phase transformation diagram is important to predict their internal phase transformation during operation (actuation). The pre-assembled (i.e., free of stress) condition represents ACTR1 at room temperature in martensite twinned phase. Upon installation, the actuator is stretched by applying an initial

stress to induce a mixture of martensite twinned and detwinned. The actuation (heating) of ACTR1 causes a phase transformation to austenite phase via an increase in both stress and temperature. This phase transformation causes the actuator to contract to its parent phase. Upon completion of actuation, ACTR1 cools down with a release of stress, and accessible

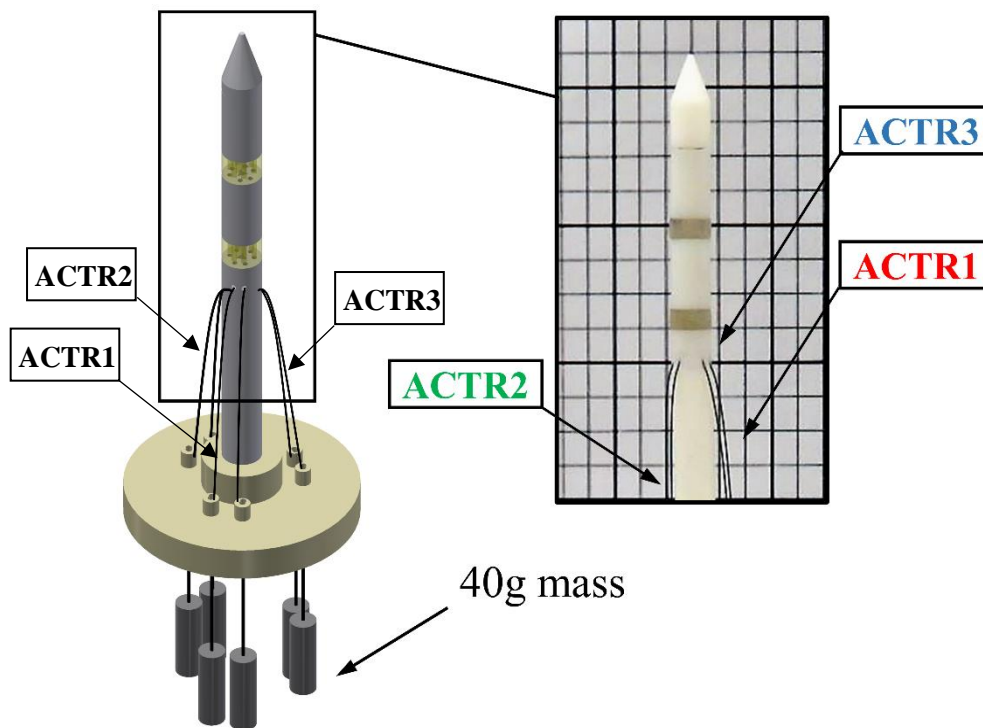


**Figure 3.2.** Schematic view of the experimental setup (left), active needle prototype with three SMA-wire actuators (right). The 40g of mass applies a total prestress of 5.55 MPa, on each SMA-wire actuator. for the next actuation cycle.

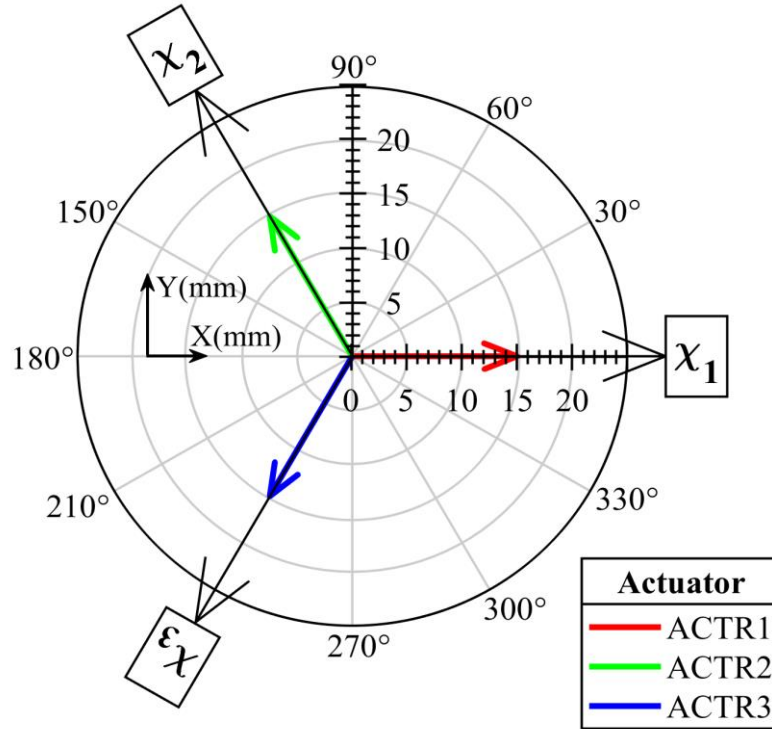
Prior to installation, ACTR2 and ACTR3 are in their martensite twinned phase. Installation of ACTR2 and ACTR3 on the active needle leaves them at a mixture of twinned

and detwinned martensite (similar to ACTR1). When ACTR1 contracts, ACTR2 and ACTR3 expand to their detwinned martensite phase to realize needle bending in the direction of ACTR1. Upon completion of actuation ACTR2 and ACTR3 return to their relaxed (free of stress) condition, ready for the next operation cycle. For more detail please refer to [50].

### **3.3. Kinematics of the Active Flexible Needle**

#### **3.3.1. Three-axis coordinate system**

Structural analysis of the 3D steerable active needle signifies the kinematic characteristics of the system. The characteristics of the system were analyzed to obtain a kinematic model for the active needle. In the kinematic model of the system, the three SMA-wire actuators were considered as three independent linear actuators. The strain in each of the SMA-wire actuators; ACTR1, ACTR2, ACTR3, when actuated, induces a deflection in the needle structure along the corresponding actuation axes of the actuators;  $\chi_1$ ,  $\chi_2$ , and  $\chi_3$ . Figure 3.3 illustrates the kinematic model concept of the active needle with three independent actuators inducing a deflection along their individual actuation axis when actuated.

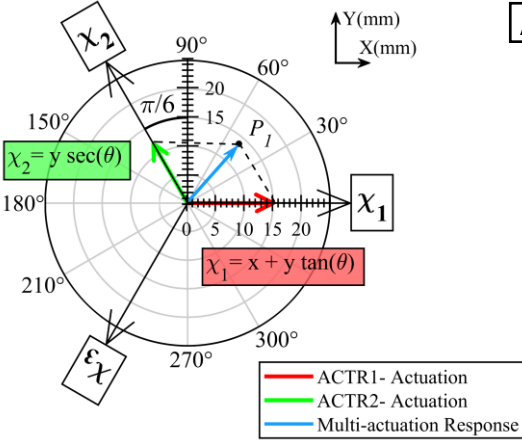
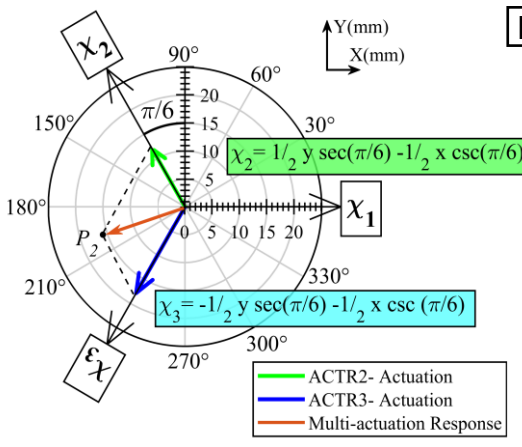


**Figure 3.3.** Kinematic model concept of the active needle with three SMA-wire actuators. The three actuators independently induce a deflection along their corresponding actuation axis  $\chi_i$ . Top view of the active needle is shown.

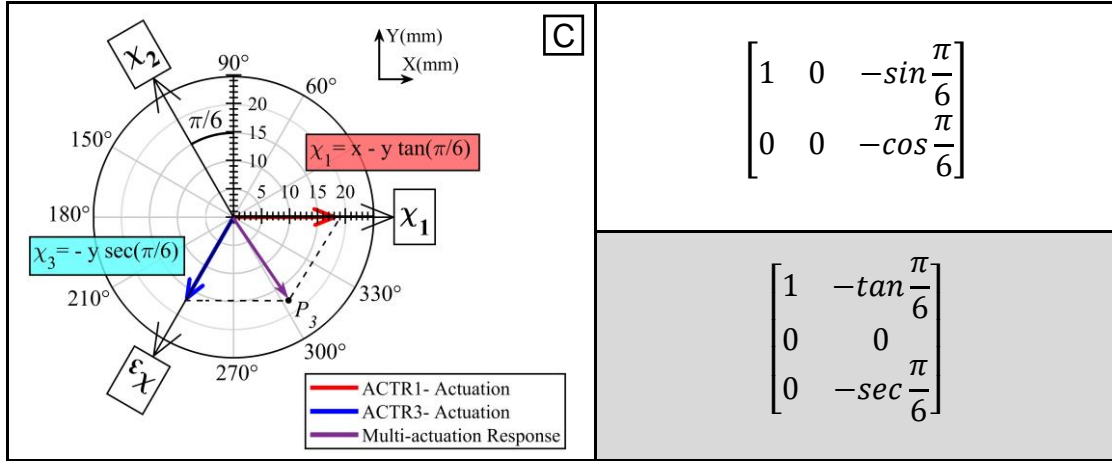
In the kinematic model of the active needle structure, Cartesian coordinates, i.e.,  $[X, Y]$ , were converted to a nonorthogonal three-axis coordinate system defined by actuation axes of the three SMA-wire actuators, i.e.,  $[\chi_1, \chi_2, \chi_3]$ . The three-axis coordinate simplifies the application of superposition principle in the kinematic model of the system to predict the deflection of the active needle in SMA multi-wire actuation systems. This way, a position vector ( $r = \overline{OP}$ ) on the XY-plane (Cartesian coordinate plane) is interpreted by vector sum of

interacting vectors directed along the actuation axes of the three SMA-wire actuators, with known magnitudes. Controlling the system's response (deflection of the active needle), to the level of the magnitude of the interacting vectors in individually controlled actuation of the SMA-wire actuators, causes a deflection equivalent to the primary position vector,  $\vec{r}$ ; by superposition principle, assuming the three SMA-wire actuators as independent linear actuators. To convert coordinates of a point,  $P(x, y)$ , in Cartesian coordinate system, to the outlined skew coordinate system with three axes, only the two neighboring  $\chi_i$  axes were taken into consideration, and the other axis was not interposed. The change of coordinate matrices for converting coordinates between the Cartesian and the three-axis skew coordinate systems is presented in Table 3.1. It also includes a graphical representation of the kinematic model, in which the  $xy$ -plane is divided into three sections each confined by two  $\chi_i$  axes, for three different multi-actuation case scenarios. It is visualized that in positioning control, positioning the needle tip between the  $\chi_1$ , and  $\chi_2$  axes does not require actuation in the direction of  $\chi_3$  axis, implying that  $\chi_3 = 0$ .

**Table 3.1.** Kinematic model concept of the active needle: system's response to multi-actuation schemes, change-of-coordinate matrices converting between the Cartesian and the three-axis skew coordinates dividing the XY-plane into three  $\frac{1}{3}$  plane zones.

<p style="text-align: center;"><b>Kinematic Modelling of the Active Needle</b> <b>in SMA Multi-wire Actuation Schemes</b></p>	<p style="text-align: center;"><b>Change-of-Coordinate Matrices</b></p>	
		<p style="text-align: center;"><i>Skew</i> <math>\rightarrow</math> <i>Cartesian</i>: <math>P_S \begin{bmatrix} \chi_1 \\ \chi_2 \\ \chi_3 \end{bmatrix} \rightarrow P_C \begin{bmatrix} x \\ y \end{bmatrix}</math></p>
		<p style="text-align: center;"><i>Cartesian</i> <math>\rightarrow</math> <i>Skew</i>: <math>P_C \begin{bmatrix} x \\ y \end{bmatrix} \rightarrow P_S \begin{bmatrix} \chi_1 \\ \chi_2 \\ \chi_3 \end{bmatrix}</math></p>
	$\begin{bmatrix} 1 & -\sin \frac{\pi}{6} & 0 \\ 0 & \cos \frac{\pi}{6} & 0 \end{bmatrix}$	
	$\begin{bmatrix} 0 & -\sin \frac{\pi}{6} & -\sin \frac{\pi}{6} \\ 0 & \cos \frac{\pi}{6} & -\cos \frac{\pi}{6} \end{bmatrix}$	
	$\begin{bmatrix} 0 & 0 \\ -\frac{1}{2} \csc \frac{\pi}{6} & \frac{1}{2} \sec \frac{\pi}{6} \\ -\frac{1}{2} \csc \frac{\pi}{6} & -\frac{1}{2} \sec \frac{\pi}{6} \end{bmatrix}$	





### 3.3.2. Translation of the SMA-wire Actuators' Strain to Needle Displacement

Motion of the active flexible needle is achieved by the direct motion of flexible joints via actuation of the SMA-wire actuators. The generated strain/stress in SMA-wire actuators exerts a force on the flexible joints causing the joints to deform elastically during the actuation duty cycles. The flexible joints (Digital Photopolymer) undergo large elastic deformations, exhibiting a nonlinear elastic material behavior, under applied stress. The deformation, i.e., change of the geometric shape, in flexible joints deflects the needle in the direction of the actuation axis of the corresponding actuator. Figure 3.4 presents a schematic illustration of the deformation in flexible joints under single SMA-wire actuation duty.

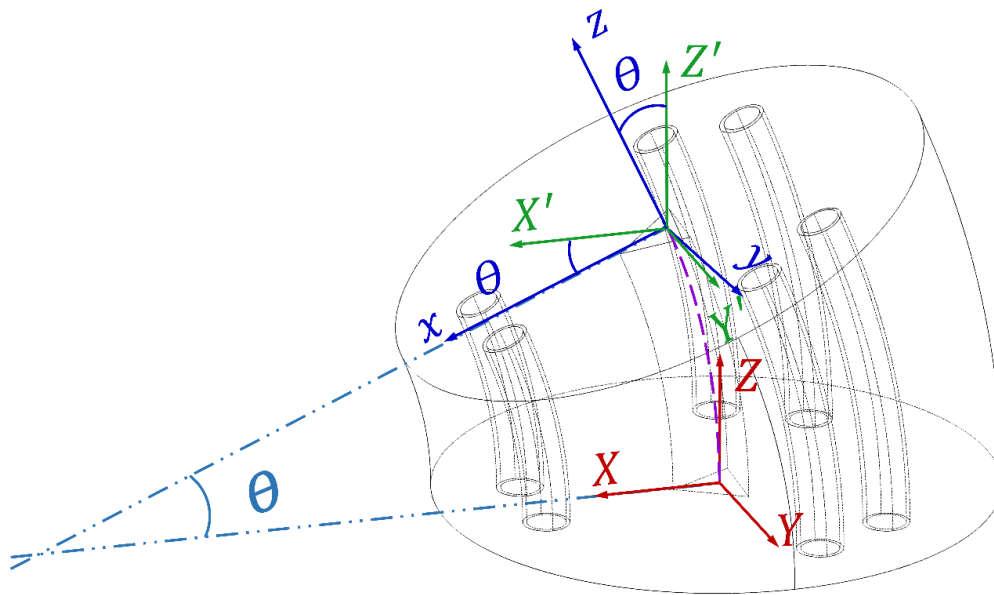


**Figure 3.4.** Deformation of the flexible joints during the actuation of SMA-wire actuators

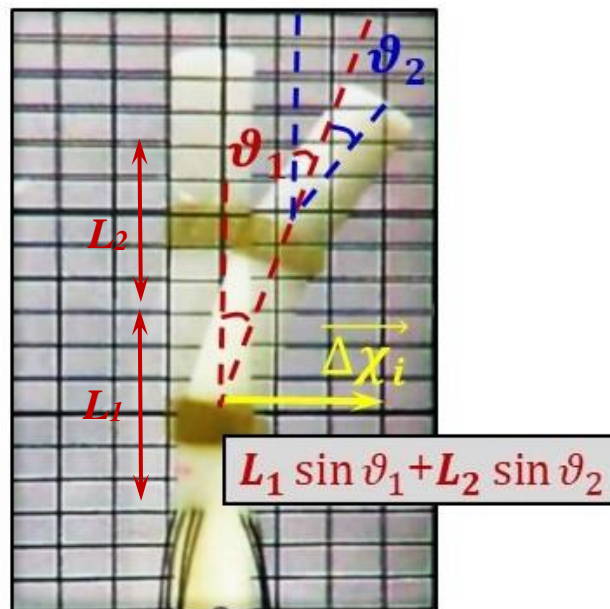


**Figure 3.5.** Kinematics characteristics of the active flexible active needle; 3DoF RR-configured manipulator.

The mechanism of the flexible active needle characterizes a three degree of freedom (3DoF) two-link RR configured manipulator. Direct motion of the flexible joints in one rotational or translational direction provides an additional DoF to the manipulator.

### **3.4. SMA Self-Sensing Electrical Resistance Feedback Control**

Manipulating the active needle and controlling the position at the needle tip demands controlled actuation of the three SMA-wire actuators. The control scheme, implemented to actuate the active needle, was designed based on the concept of *smart actuation* (explained in Section 1.2). The control system actuates the SMA-wire actuators, controlling the amplitude of the input electric current actuation signals, while taking online measurements of the electric current and voltage across the SMA-wire actuators to monitor the electric resistance and the supplied electrical power using *ohm's law*, for the three SMA-wire actuators. The computer control system derives online estimates of the actuator position (strain) by assessing the strain-power-resistance characteristics mapped data.

The control system regulates the Amplitude of the electric current input signal to actuate and control the SMA-wire actuators. The high amplitude electric current signal serves as the actuation heating cycle, delivering electrical power to actuate the SMA-wire actuators (*Joule* heating); while the low amplitude electric current signal is a low nonzero amplitude

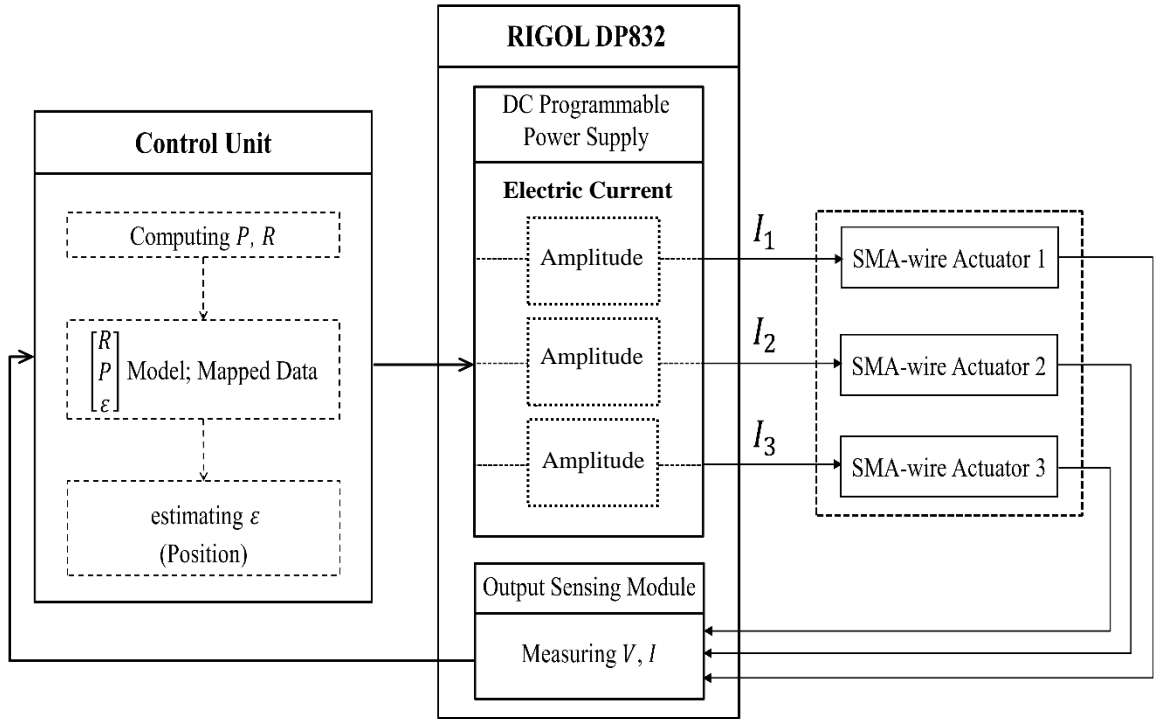


**Figure 3.6.** Control system architecture: multi-actuation and self-sensing electric resistance feedback control of multiple SMA-wire actuators.

signal serves as the actuation cooling cycle due to the higher rate of cooling by natural convection compared to the power generation by the low amplitude electric current signal in SMA-wire actuator. The low amplitude current signal was intended to prevent singularities in measuring the electric resistance of the SMA-wire actuators by *ohm's law*;  $\lim_{i \rightarrow 0} R = \infty$ . The control system exploits self-sensing capabilities of SMA-wire actuators; taking the real-time measurements of the electric resistance ( $R$ ) and electric power ( $P$ ) of the SMA-wire actuators, in tunable time intervals ( $T_D$ ), to obtain online estimations of the actuators displacement by the assessments of the actuators numerically mapped strain-power-

resistance characteristics data. The electric power is measured to determine the current state of the actuation duty, i.e., heating and cooling cycles. Measuring the electric resistance, due to the hysteresis in SMAs, measuring the electric resistance does not reveal the current state in heating or cooling paths in actuation duties. The control system architecture is presented in Figure 3.6.

### **3.5. Tracking System**

Vision-based tracking is the method used for position tracking of the active needle tip. Position tracking was performed by image processing in MATLAB using MATLAB Image Acquisition Toolbox™, and MATLAB Computer Vision Toolbox™. The video images were captured using a Canon PowerShot SX60 HS camera with a 3.8-247.0mm 1:3.4-6.5 USM lens at 30fps frame rate, during the actuation. The algorithm for the image processing detects a set of feature points inside a user-defined interest region in the image. While reading the frames, for the identified set of feature points in the previous frame, the tracker attempts to find the corresponding point in the current frame. Then estimates the translation, rotation, and scale between the previous and the current points.

## **Chapter 4**

### **Results and Discussions**

The main goal of this study is to realize a desired deflection at the 3D printed needle prototype via actuation of multiple SMAs, without a need for an external position sensor in a feedback control algorithms. This chapter first explains the characterization of the active 3D printed needle prototype in response to actuation of multiple SMAs in Section 4.1. Then Section 4.2 explains the shape-sensing capabilities of the SMAs, and feedback control of the active needle prototype.

#### **4.1. Characterization of the 3D Steerable Active Needle with Multiple Interacting SMA-wire Actuators**

Characterizing the response of SMA-actuated dynamical structures to actuation in terms of deflection (displacement) in their structure, coupled with variations of the electric resistance of the SMA-wire actuators in actuation on account of applied electric power (heat generation) is critical to determine the required material parameters in generating reliable models of the system, or the system components, e.g., actuators. Characterization is the primary step towards the tracking and motion control of active navigating devices in model-based control applications.

### 4.1.1. Characterization of the Active Flexible Needle Response to Actuation

Experimental characterization of the active needle in response to a variety of applicable actuation schemes was performed to characterize the electric power and variations of the actuator's electric resistance and strain (with respect to needle deflection). A constant electric current signal was applied to actuate the SMA actuators, delivering the electric power to the actuators over actuation duty cycles. The actuation signal used in characterization experiments is shown in Figure 4.1.

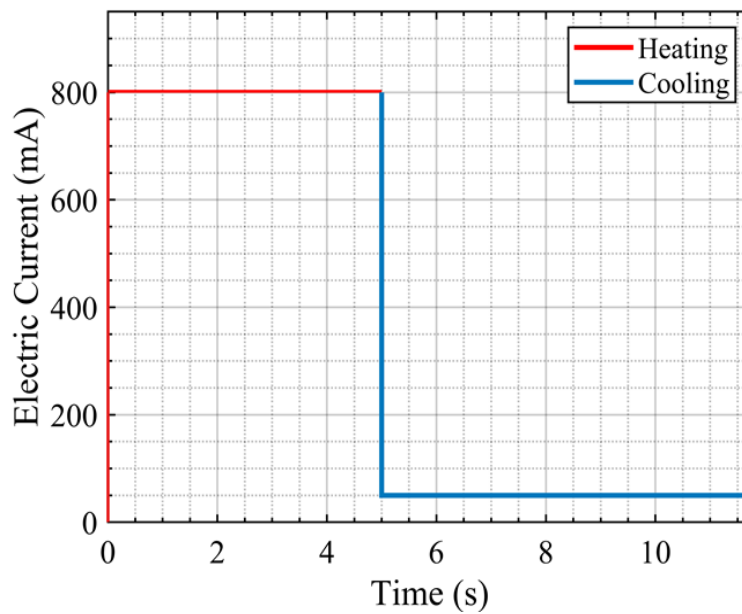


**Figure 4.1.** Electric current: SMA-wire actuation signal in characterization experiments.

It should be noted that the electrical current in the cooling cycle was set at a small non-zero amount (i.e., 50mA). This is for the controller to predict and keep track of the internal phase of the SMAs during cooling cycle via electrical current, voltage and electrical resistance of the SMA wires. Details are explained in Section 4.2.

The electric current input was selected to induce a complete phase transformation ( $\xi: 1 \rightarrow 0$ ) in the SMA-wire actuators in 5 seconds. This limitation was to prevent overheating and loss of shape memory effect in the SMA-wire actuators. The maximum level of the electric current signal that could be applied to the wires depends on the required level of actuation and signal duration. For instance, the amplitude of the electric current signal for a complete phase transformation of the SMA-wire actuators (0.29mm diameter size) in 1 second is approximated as 1500mA in Flexinol® datasheet by ©Dynalloy, Inc. It should be noted that the 800mA electric current input signal applied in this work mitigates the risk of overheating the SMA-wire actuators, yet induces a complete phase transformation in about 5 seconds; making a trade-off between operation safety and actuation time.

In the first set of characterization experiments, mechanical characteristics of the flexible structure of the active needle was tested in single SMA-wire actuation duties where each of the three SMA-wire actuators; ACTR1, ACTR2, and ACRT3 was actuated separately. The induced strain in the SMA-wire actuators impels the flexible structure of the active needle to deflect causing a displacement in the position at the needle tip. Figure 4.2



shows the top and front view of the deflection in the needle structure under single wire actuation duties.

Position of the active needle at the needle tip was tracked in three-dimensional (3D) space

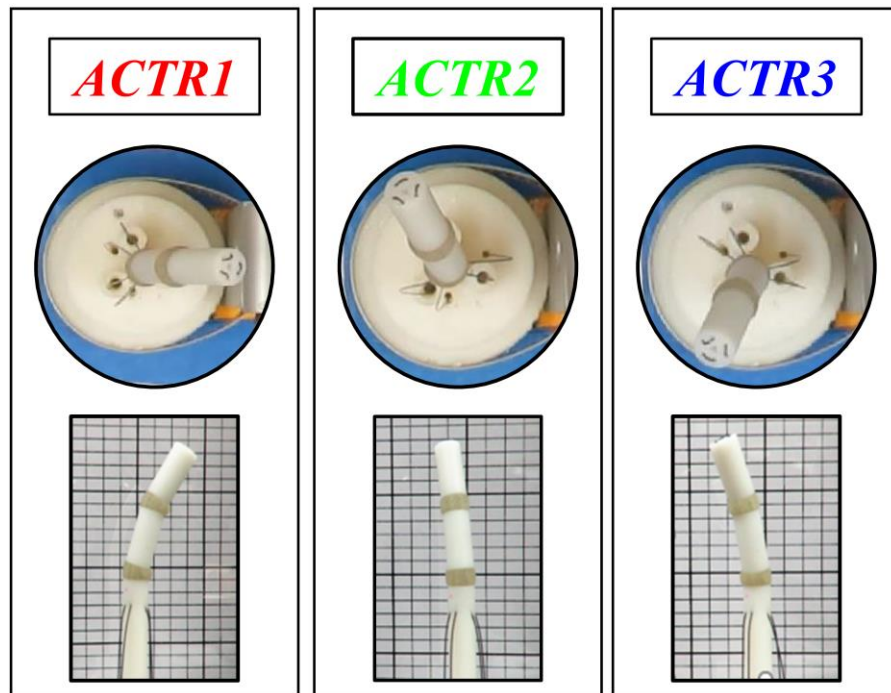


**Figure 4.2.** Deflected shape of the active needle prototype under single SMA-wire actuation in direction of each SMA actuator.

$(X, Y, Z)$  during the actuation of the three SMA-wire actuators using computer vision-based position tracking method. Results are illustrated in Figure 4.3. It should be noted that the needle tip moves in the direction of  $X$  and  $Y$  upon actuation of ACTR1 and ACTR2, respectively, while negligible movement in  $Z$  direction. Actuation of ACTR3 realizes movement only in

Y direction since the Y axis (in the coordinate system adopted) pointing from the centre to the ACTR3, and thereby negligible movement in X and Z directions.

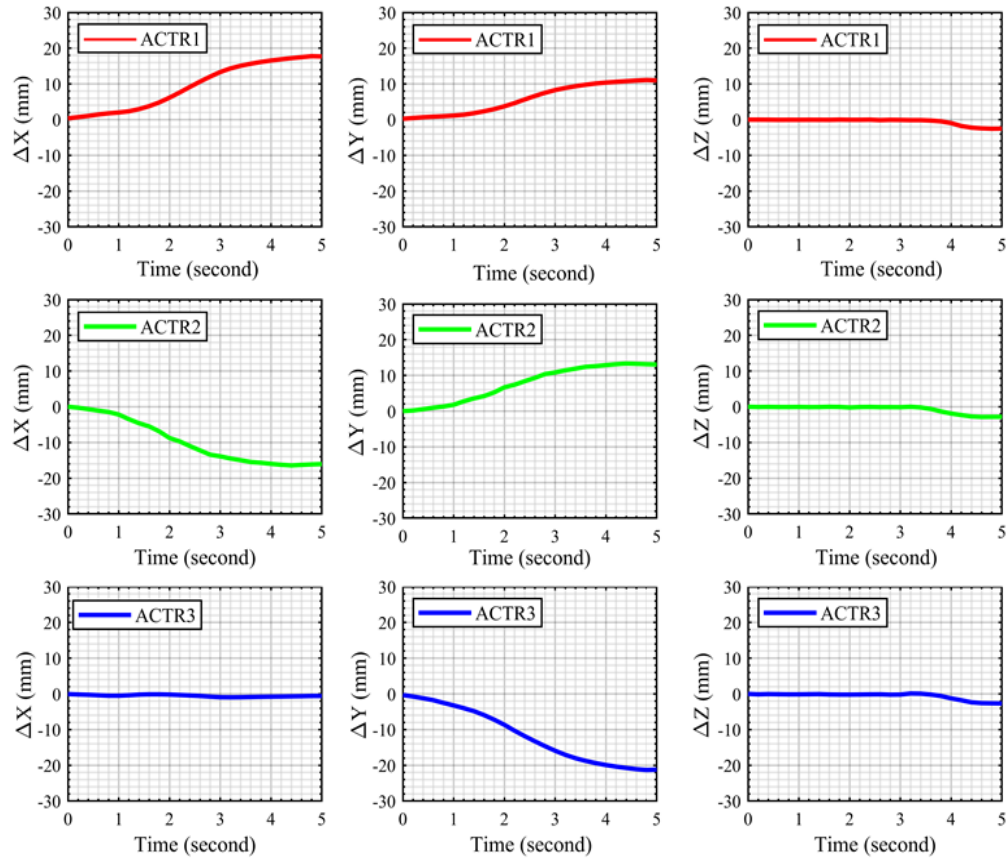


**Figure 4.3.** Position tracking (3D displacement measurement) of the active needle tip under single actuation duty cycles for the three SMA-wire actuators; ACTR1, ACTR2, and ACTR3.

In addition to single actuation schemes, the multi-actuation schemes in which multiple actuators are actuated in parallel, was implemented to actuate three interacting SMA-wire

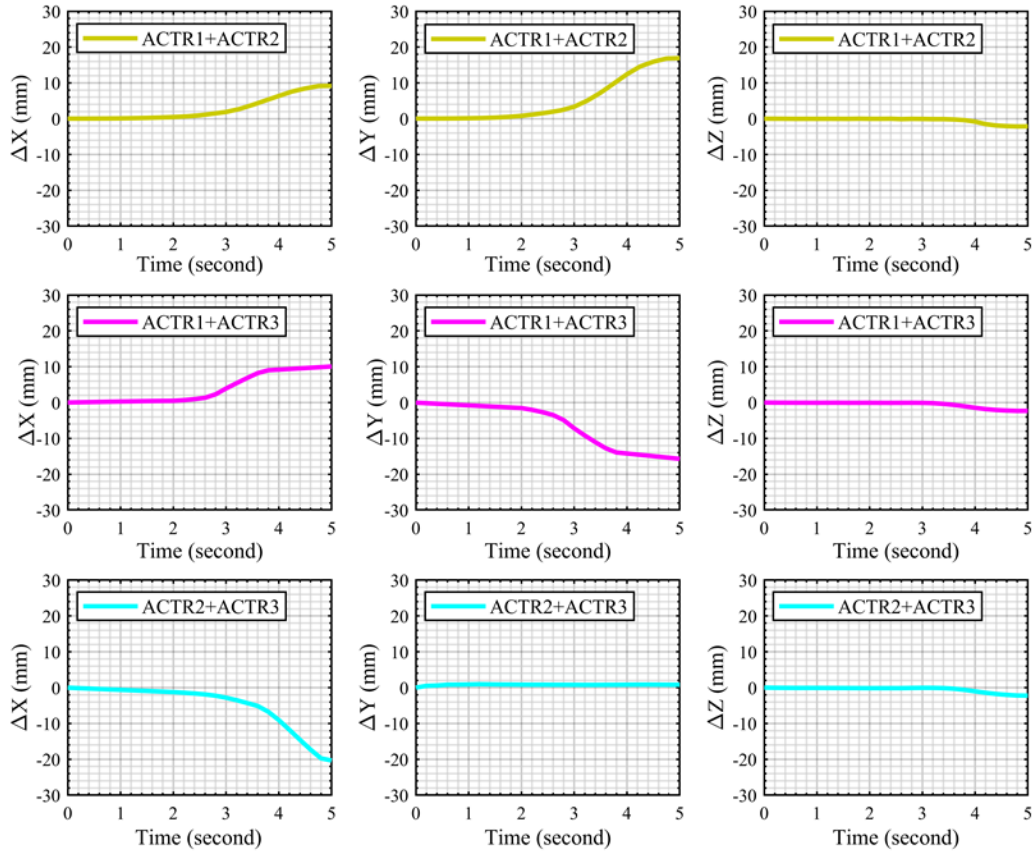


**Figure 4.4.** Position tracking (3D displacement measurement) of the active needle tip under dual actuation duty cycles; parallel actuation of pair sets of the three SMA-wire actuators; {ACTR1, ACTR2}, {ACTR1, ACTR3}, and {ACTR2, ACTR3}.

actuators to manipulate the active needle. In this set of characterization experiments, mechanical characteristics of the flexible structure of the active needle was tested under dual SMA-wire actuation duties where two of the three SMA-wire actuators; ACTR1, ACTR2, and ACTR3, were actuated synchronously. Position at the needle tip was tracked in 3D space ( $X, Y, Z$ ) during the actuation. Figure 4.4 illustrates the displacement in position of the active

needle at the tip under the dual actuation duties. In dual actuation duties, pair sets of the three SMA-wire actuators; {ACTR1, ACTR2}, {ACTR1, ACTR3}, and {ACTR2, ACTR3} were actuated concurrently. It should be noted here that dual actuation of {ACTR2, ACTR3} realizes movement only in X direction because of the fact that vector summation of the vectors pointing from the centre to the ACTR2 and ACTR3 lies on the X axis (of the coordinate system), and thereby negligible movement in Y and Z directions.

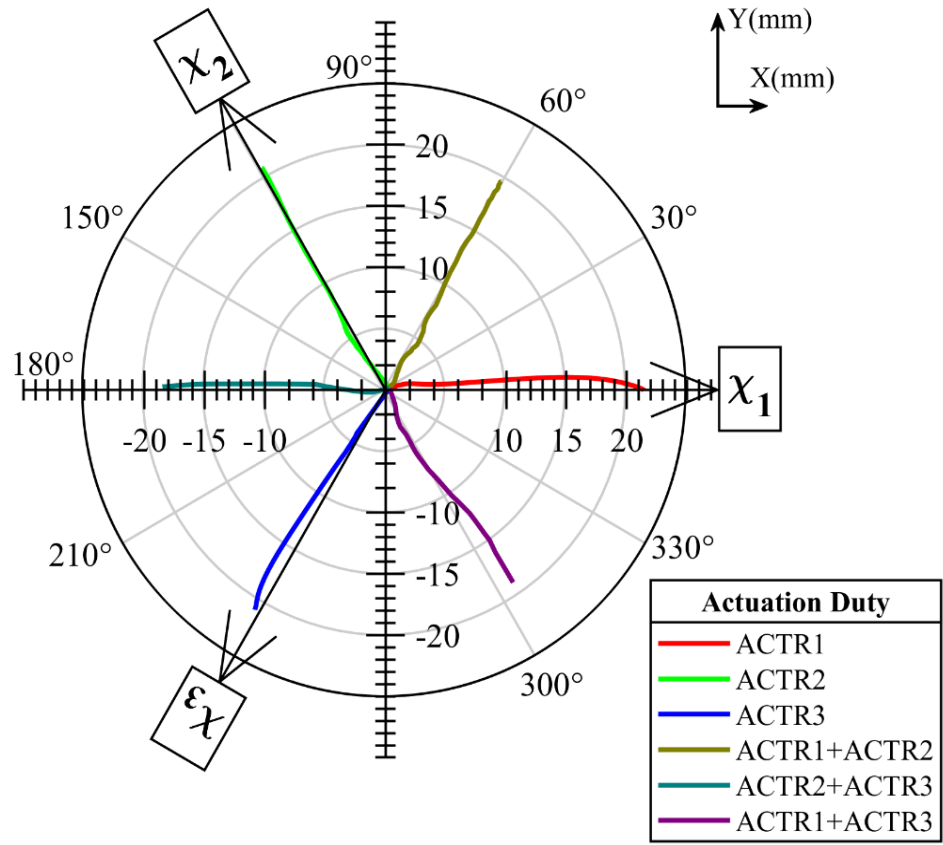


**Figure 4.5.** Travel path of the active needle; position of the needle at the tip in XY-coordinates (Cartesian coordinate system) under single and dual actuation duties.

The dual actuation scheme unlocks additional set of points in 3D space that are within reach of the needle tip, leading to an increased workspace volume of the active needle. Figure 4.5 illustrates the XY-coordinates of the motion paths of active needle (travel path of the needle tip) in single and dual actuation schemes for the triple set of SMA-wire actuators.

Figure 4.5 visualizes the motion paths (position vector) of the needle tip in response to the multi-actuation scheme, i.e., dual actuation duties of the pair sets of the SMA-wire actuators. The position vectors were equivalent to the resultant (vector sum) of the motion paths (position vectors) of the needle tip in response to single actuation duties of the corresponding actuators of that pair set. This signifies the potential to realize active 3D steering of the triple SMA-actuated active needle (rigid links, and elastic joints) by means of precise actuation schemes; implemented in conjunction with efficient control approaches, to drive the SMA-wire actuators. This was verified in a set of experiments where the self-sensing, resistance-based feedback control algorithm controls the input electrical actuation signals of the three SMA actuators for the task of path following. The Results, including characterization of SMA-wire actuators, and multi-actuation control of a triple SMA-actuated system for the task of path following are presented in the following section. The active needle with the flexible structure design and the triple SMA-wire actuator configuration, manipulated in multi-actuation mode, can reach target points with X and Y coordinates (XY-plane) within the radius of 20mm in 3D space. The Z-displacement, however, is limited, and is only in one direction (downward). Figure 4.6 illustrates the 3D workspace of the active needle.

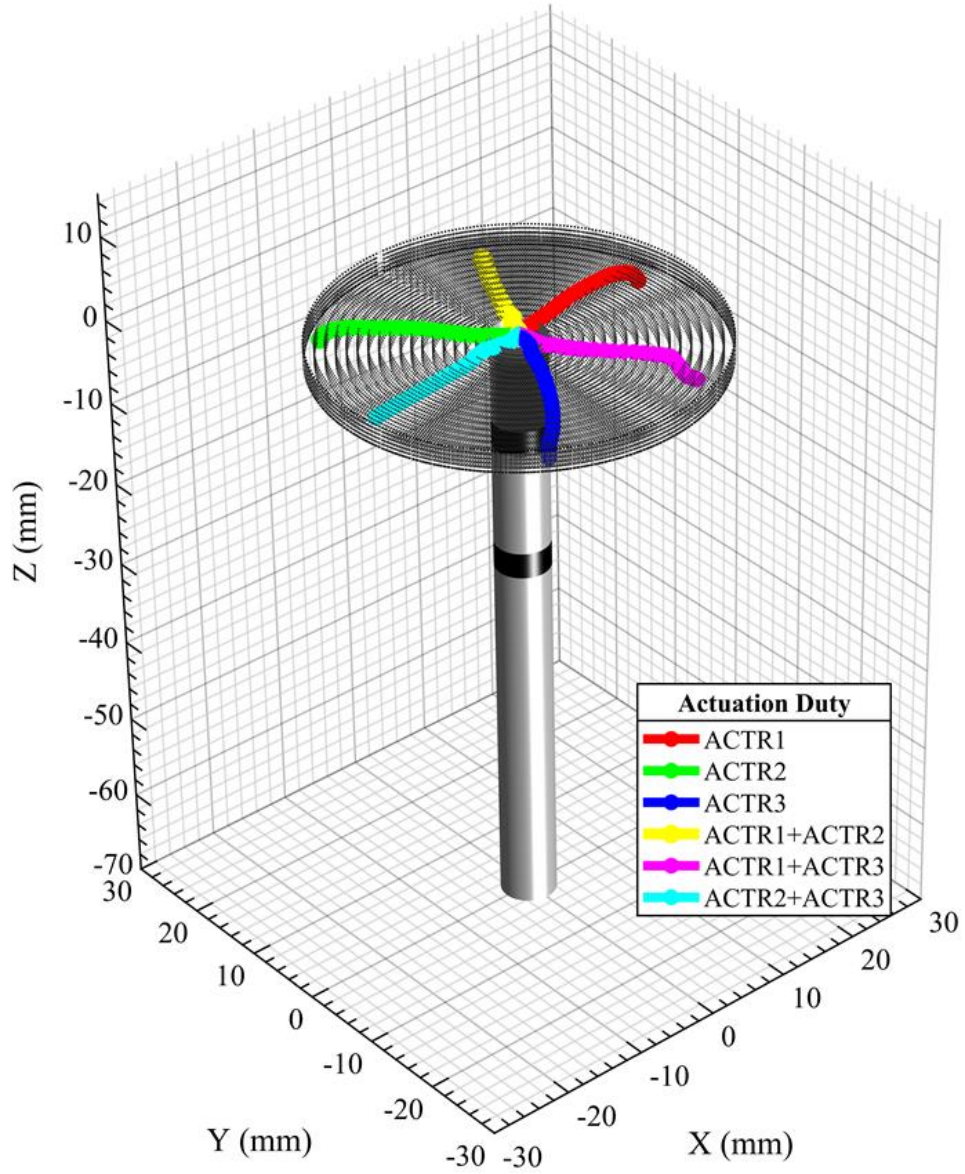


**Figure 4.6.** 3D spatial workspace of the active needle; multi-actuation of the SMA-wire actuators in parallel enables manipulation of the active needle to place the tip at target points within 20mm radial distance on XY-plane.

#### **4.1.2. SMA-wire Actuator Characterization**

Characterization of the SMA-wires in terms of actuator's strain and electrical resistance is a critical step to exploit self-sensing characteristics and sensor functionality of SMA actuators. Electrical resistance of an SMA wire varies by the fraction concentration of the present phases, i.e., austenite and martensite, in the material, and changes measurably during the phase transformation. In addition, the strain in an SMA-wire actuator is a function of the volume fraction concentration for the martensite and austenite phases present in the material during the phase transformation. Consequently, the strain and the electrical resistance in an SMA-wire are correlated. The strain-resistance correlation in the SMA wires conveys their unique self-sensing capabilities and provides the scope for a sensor-less control system adopting the SMA-wire actuator as position sensors by measuring their electrical resistance. The strain-resistance correlation, obtained from characterization experiments, was applied to develop mapping functions that relate the system output (i.e., position of the end effector) to the temperature-induced strain in SMA-wire actuator and its electrical resistance at different actuation levels. Characterizing the response of SMA-wire actuators and their correlated strain-resistance behavior contributes to constructing system models and designing control systems with internal resistance feedback to control SMA-wire actuators.



To characterize the response and quantify the strain-resistance correlated behavior of SMA-wire actuator, the electric current and voltage across the SMA-wire actuator was measured during the actuation, and the electrical resistance of the SMA wire is calculated using ohm's law. The thermodynamic equilibrium (Eq. 1) defines the temperature of an SMA wire, in the course of Joule heating actuation, as a function of the input electrical power, heat conduction between the martensite phase at a low temperature and a phase at a higher temperature (martensite or austenite) due to the latent heat of phase transformation, and the heat convection to the ambient. It is denoted that the input electrical power directly impacts the temperature of the SMA wire [101]. Hence, the strain-resistance response of the SMA wire was characterized in terms of the electrical power input to the system. The results presented in Figures 4.7 - 4.9 illustrate the electrical resistance variations in the three SMA-wire actuators; ACTR1, ACTR2, and ACTR3.

Characterization of the SMA actuation response to define a self-sensing feedback model (i.e., strain-resistance relationship) was implemented by curve fitting on the experimental data with cubic polynomials.

It should be noted that SMA characterization in this case was done on the SMA-wire actuators fully attached to the active needle. Thereby, actuation imposed a change in stress level during operation. Considering that the electrical resistance is a function of both stress and strain, the trend seen in Figures 4.7- 4.9 can be explained by the increasing coupling

force(s) due to deformation of inactive SMA-wire actuator(s) at low-temperatures. The heating and cooling processes are shown in the figures.

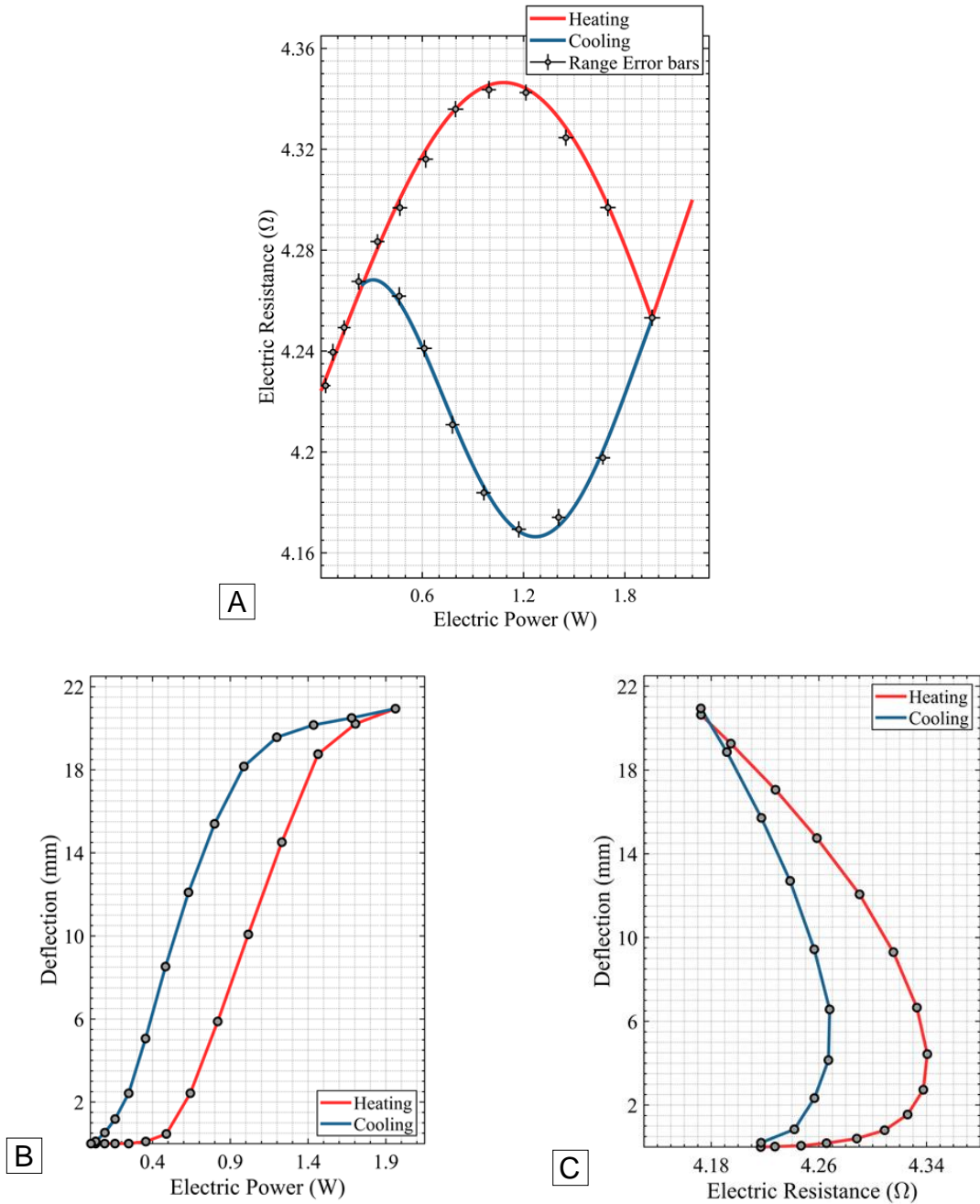


**Figure 4.7.** SMA-wire actuator self-sensing characteristic; electric resistance vs. electric power, and mapping the active needle response to SMA-wire characteristics. The data was obtained with three repetitions on the wires (note small error bars); **B.** needle deflection vs. electric power, **C.** needle deflection vs. electric resistance, for **ACTR1**.

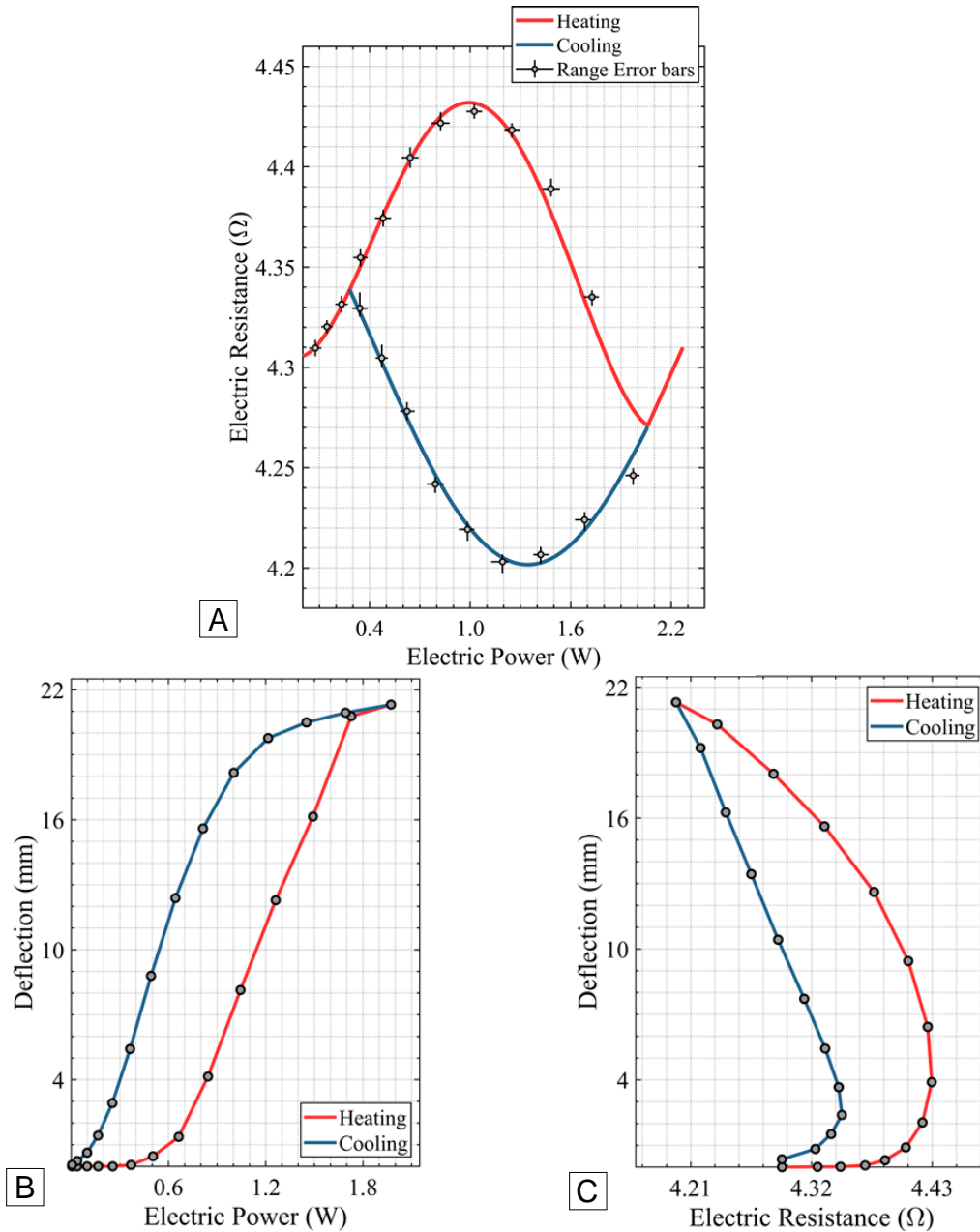


**Figure 4.8.** SMA-wire actuator self-sensing characteristic; **A.** electric resistance vs. electric power, and mapping the active needle response to SMA-wire characteristics. The data was obtained with three repetitions on the wires (note small error bars); **B.** needle deflection vs. electric power, **C.** needle deflection vs. electric resistance, for **ACTR2**.

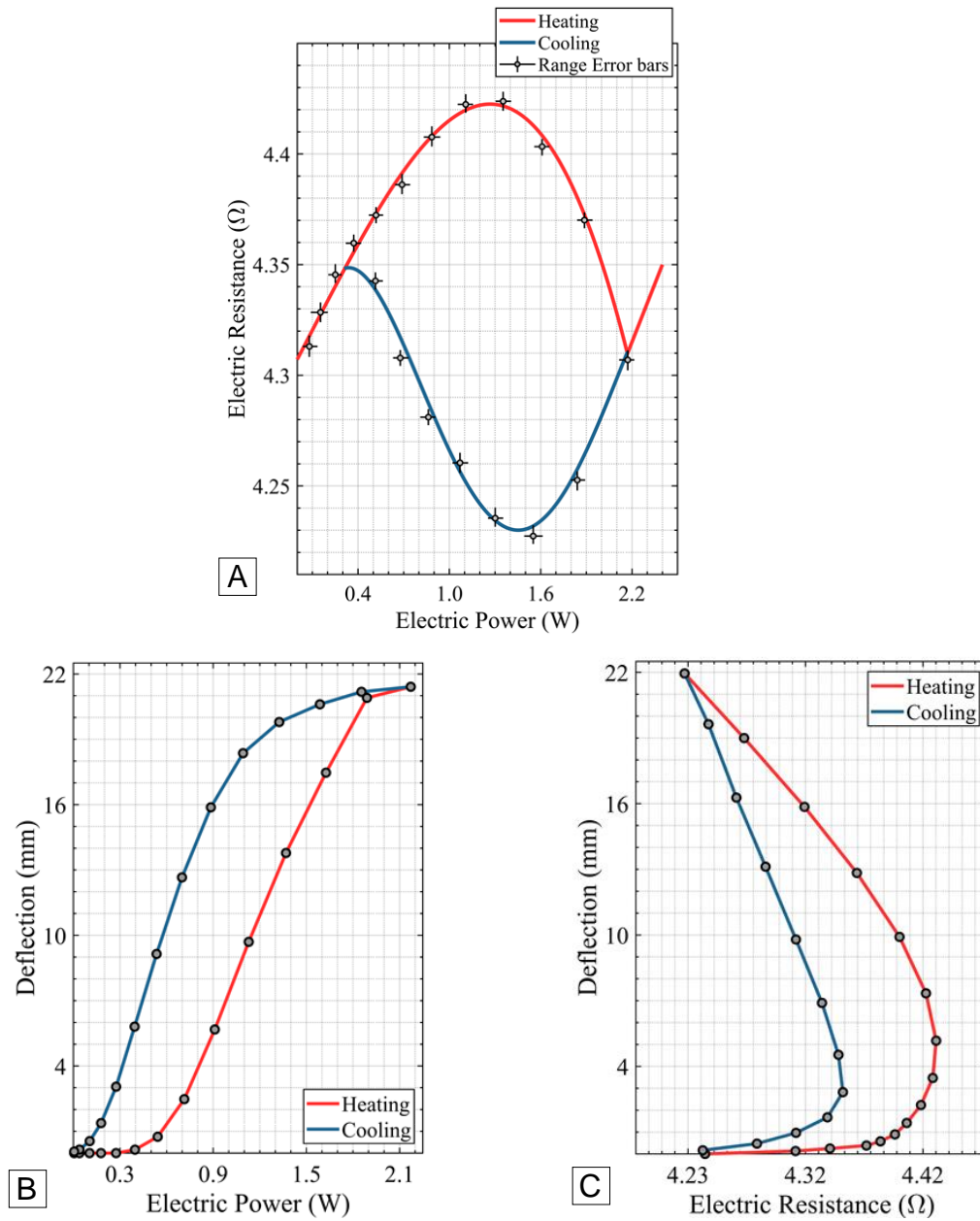


**Figure 4.9.** SMA-wire actuator self-sensing characteristic; **A.** electric resistance vs. electric power, and mapping the active needle response to SMA-wire characteristics. The data was obtained with three repetitions on the wires (note small error bars); **B.** needle deflection vs. electric power, **C.** needle deflection vs. electric resistance, for **ACTR3**

## **4.2. SMA Self-Sensing Electrical Resistance Feedback Control**

The control system was primarily tested on a single SMA-wire actuator to verify the performance of the self-sensing resistance feedback control system in tracking control. The results for tracking control of the single SMA-wire actuator and the SMA-based multiactuator flexible active device with self-sensing resistance feedback are presented in the following sections.

### **4.2.1. Tracking Control of a Single SMA-wire Actuator**

The control system performance was tested in position control of a single SMA-wire ( $l = 50\text{cm}$ ,  $d = 0.29\text{mm}$ ) actuator (©DYNALLOY, Inc.), and the test results are presented in Figures 4.10- 4.11. The control system was intended to manipulate the single SMA-wire actuator to track a contraction between 0-20mm at 5mm steps. The control system regulates the amplitude of the input electric current actuation signal. Figure 4.10 illustrates the strain-resistance characteristics of the SMA-wire actuator acquired in experimental implementations. A 300g of mass attached to the SMA-wire actuator applies a total stress of 44.54 MPa.

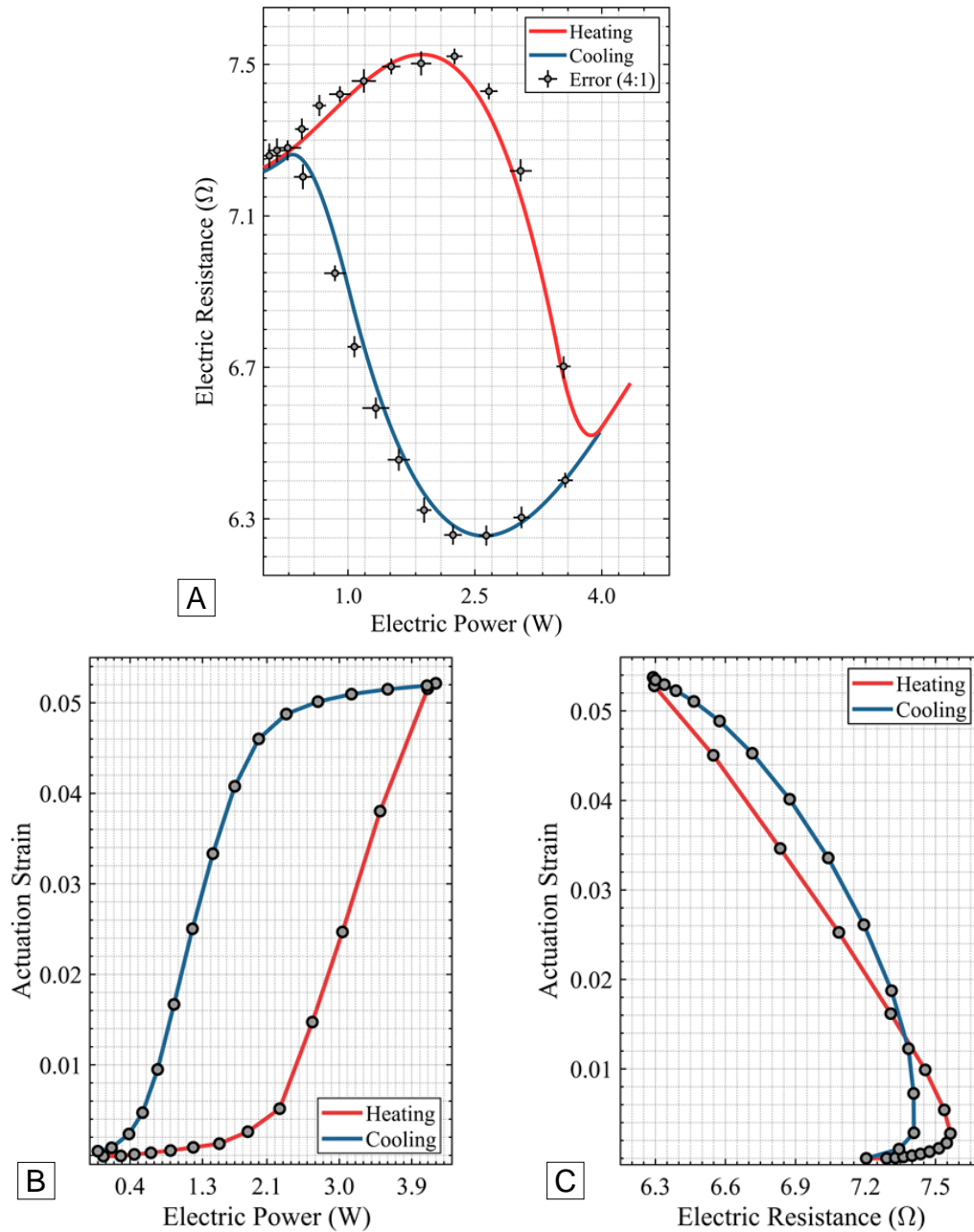


**Figure 4.10.** SMA-wire actuator self-sensing characteristic: **A.** electric resistance vs. power, and mapping the response characteristics of the SMA-wire; The data was obtained with three repetitions on the wires (note small error bars); **B.** deflection (actuation strain) vs. electric power, **C.** deflection (actuation strain) vs. electric resistance for the SMA-wire under tension.

Figure 4.11 illustrates the single SMA-wire actuator response ( $\Delta Y$ ) under the self-sensing electrical resistance feedback control signal. Absolute and relative positioning errors in tracking control of the SMA-wire actuator of less than 4mm, and 8mm were found, respectively. The controller parameters were set to  $I_H = 0.99 A$ ,  $I_L = 0.05 A$ ,  $T_D = 200 ms$ .



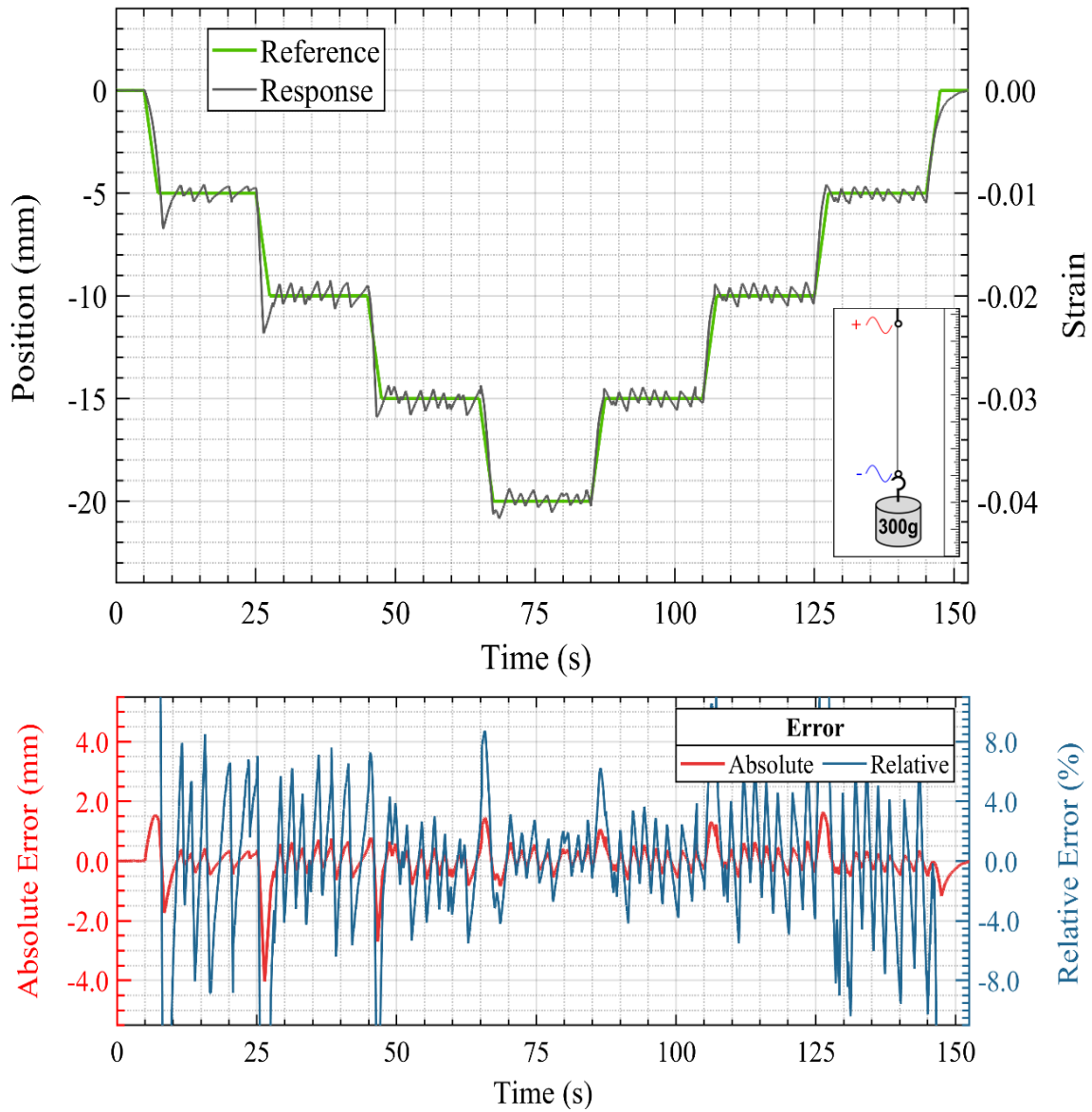


**Figure 4.11.** Control system performance in position tracking of a single SMA-wire actuator: tracking reference and response of the SMA-wire (top) and tracking error (bottom).

#### 4.4.2. Tracking Control of the 3D Steerable Active Needle via Control of Multiple Interacting SMA-Wire Actuators

The control scheme was implemented on the triple set of interacting SMA-wire actuators to control the active needle. Manipulating the active needle tip to track a desired path required accurate controlled actuation of three interacting SMA-wire actuators. The performance of the self-sensing electric resistance feedback control system in manipulating the needle tip for path tracking was tested and the results are presented in Figure 4.12. The reference path was a vertical path (in Cartesian coordinate system; Y-axis) with the start point  $P_1(0,0)$ , and the end point  $P_2(0,15)$ . Figure 4.12 illustrates the needle trajectory, and the active needle response (position at the needle tip) under control actuation signals in the path tracking control. The control parameters of the controller are set as  $I_H = 0.65$ ,  $I_L = 0.05$ , and  $T_D = 100$  ms.

The tracking control system, developed in this work, has resulted in an absolute error of less than 1mm in a radial tip displacement of 15mm (please see Figure 4.12). The absolute error was larger at larger needle tip displacements, whole more accurate at small tip displacements. Position tracking error (Figure 4.11) has also shown an absolute error of less than 2mm, except in the beginning of the control process (error of about 4mm). The absolute error reported in this work lies in the acceptable range of error (i.e., 2.7mm) in needle tip placements reported in [33] in needle-based procedures.

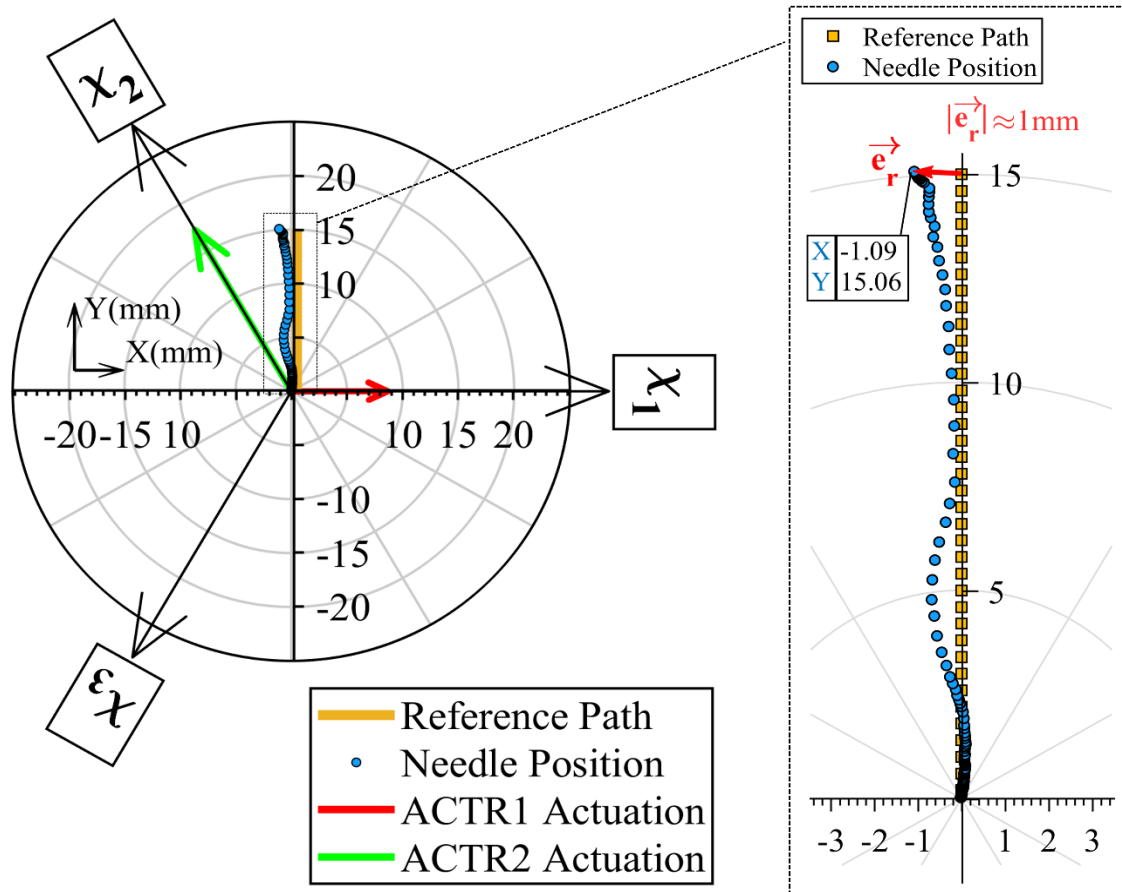
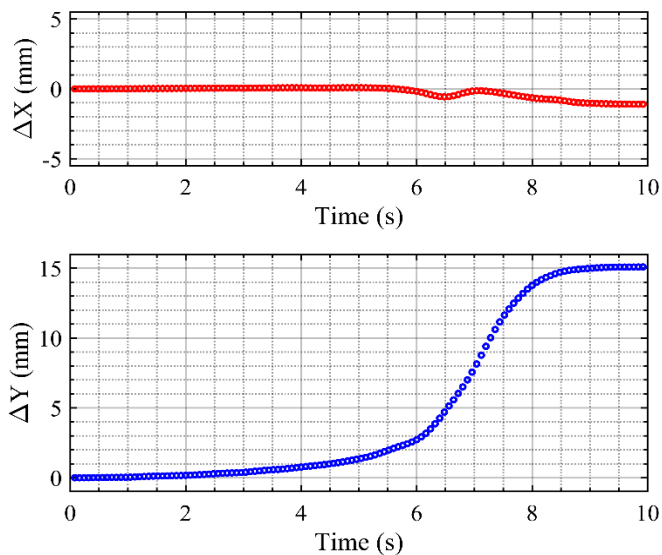


**Figure 4.12.** Reference tracking control (position control) of the active needle at the tip, under multi-actuation duties; controlled actuation of the actuators ACTR1, and ACTR2, for a reference path following task; following the straight vertical line path (yellow line).



## **Chapter 5**

### **Conclusion**

This work demonstrated controlled manipulation of a 3D steerable active needle via actuation of multiple interacting SMA-wire actuators. Developing an active needle that responds accurately to the SMA actuation is a challenging task due to the SMA's complex electromechanical behaviour, which is nonlinear, hysteresis, and history dependent. The design specifications of the active needle with rigid links and soft joints for the structure and the triple SMA-wire actuator configuration introduces additional complexity to the system for an accurate control and precise manipulation, as the three SMA-wire actuators interact actively or passively with each other in the course of actuations.

A control scheme to operate the SMA-wire actuators was designed and tested based on the concept of smart actuation. The control system takes advantage of self-sensing ability in SMA-wire actuators to estimate the position through a feedback loop based on the electric resistance of the actuator. The electrical resistance feedback loop provides an estimation of current position enabling the position control of the SMA-wire actuators with relative error of less than 10%. The control scheme offers significant advantages for small structures operating in a small space by reducing the number of system components and eliminating the necessity for an external sensing element. In addition, the control scheme was implementable

in real-time for the control applications demanding online monitoring of the state of the system. The source-controlled actuation signals control signals driving the SMA-wire actuators, optimize the energy consumption efficiently. Furthermore, the control system demonstrated to successfully manipulate the flexible structure of the active needle to track a reference path.

The contribution of this work relies on its accurate manipulation of the needle tip in 3D space, while using SMA actuators as actuators as well as position sensors. This eliminates the need for an external position sensor in feedback loop control systems. The absolute error reported in this work (i.e., less than 1mm in tip displacements of up to 25mm, and less than 2mm in position tracking) is within the acceptable accuracy (i.e., less than 2.7mm) for majority of needle-based procedure.

In summary, this work introduced an approach to control a 3D steerable active needle for surgical procedures. The triple SMA-actuated active needle and the control system demonstrated to deliver a controllable motion at the needle tip. In conclusion, the active needle and control strategy, presented in this study, showed the needle's ability to sense its shape, providing significant benefits in visualizations and tip tracking in minimally invasive surgeries. Tip tracking (provided by shape sensing capability of the active needle) eliminates the need for an additional sensor and may avoid the need for 3D imaging by combining 2D images with needle shape sensing.

## References

- [1] G. Dogangil, B. L. Davies, and F. Rodriguez Y Baena, "A review of medical robotics for minimally invasive soft tissue surgery," *Proceedings of the Institution of Mechanical Engineers, Part H: Journal of Engineering in Medicine*. 2010.
- [2] N. J. van de Berg, D. J. van Gerwen, J. Dankelman, and J. J. van den Dobbelsteen, "Design Choices in Needle Steering—A Review," *Mechatronics, IEEE/ASME Trans.*, vol. 20, no. 5, pp. 2172–2183, 2015.
- [3] M. Scali, T. P. Pusch, P. Breedveld, and D. Dodou, "Needle-like instruments for steering through solid organs: A review of the scientific and patent literature," *Proc. Inst. Mech. Eng. Part H J. Eng. Med.*, vol. 231, no. 3, pp. 250–265, 2017.
- [4] R. J. Webster, J. Memisevic, and A. M. Okamura, "Design considerations for robotic needle steering," in *Proceedings - IEEE International Conference on Robotics and Automation*, 2005.
- [5] B. Konh, M. Honarvar, and P. Hutapea, "Design optimization study of a shape memory alloy active needle for biomedical applications," *J. Med. Eng. Phys.*, vol. 37, no. 5, pp. 469–477, 2015.
- [6] L. Frasson, F. Ferroni, S. Y. Ko, G. Dogangil, and F. Rodriguez y Baena, "Experimental evaluation of a novel steerable probe with a programmable bevel tip inspired by nature," *J. Robot. Surg.*, 2012.
- [7] J. L. Ochsner, "Minimally invasive surgical procedures," *Ochsner J.*, vol. 2, no. 3, p. 135, 2000.
- [8] M. Tonutti, D. S. Elson, G. Z. Yang, A. W. Darzi, and M. H. Sodergren, "The role of technology in minimally invasive surgery: State of the art, recent developments and

future directions,” *Postgraduate Medical Journal*. 2017.

- [9] S. Karimi, B. Konh, and E. Seidi, “Towards the development of a triple SMA actuated vertical tube,” *Proc. SPIE - Int. Soc. Opt. Eng.*, vol. 10595, no. March, p. 105953D:1-5, 2018.
- [10] M. J. Mack, “Minimally invasive and robotic surgery,” *J. Am. Med. Assoc.*, 2001.
- [11] J. H. Palep, “Robotic assisted minimally invasive surgery,” *Journal of Minimal Access Surgery*. 2009.
- [12] V. Vitiello, S. L. Lee, T. P. Cundy, and G. Z. Yang, “Emerging robotic platforms for minimally invasive surgery,” *IEEE Rev. Biomed. Eng.*, 2013.
- [13] S. Karimi and B. Konh, “3D Steerable Active Surgical Needle,” in *Proceedings of the 2019 Design of Medical Devices Conference. 2019 Design of Medical Devices Conference.*, 2019.
- [14] G. G. Hamad and M. Curet, “Minimally invasive surgery,” *American Journal of Surgery*. 2010.
- [15] V. Panebianco, F. Barchetti, G. Manenti, T. Aversa, C. Catalano, and G. Simonetti, “MR imaging-guided prostate biopsy: technical features and preliminary results,” *Radiol. Medica*, 2015.
- [16] M. Muntener *et al.*, “Magnetic resonance imaging compatible robotic system for fully automated brachytherapy seed placement,” *Urology*, 2006.
- [17] A. Zivanovic and B. L. Davies, “A robotic system for blood sampling,” *IEEE Trans. Inf. Technol. Biomed.*, 2000.

- [18] T. M. Halaszynski, V. Kurup, and D. Souzdalnitzski, "Needle visualization in ultrasound-guided regional anesthesia: Technological challenges and educational solutions," *Regional Anesthesia and Pain Medicine*. 2009.
- [19] S. Pandya, J. W. Motkoski, C. Serrano-Almeida, A. D. Greer, I. Latour, and G. R. Sutherland, "Advancing neurosurgery with image-guided robotics: Technical note," *J. Neurosurg.*, 2009.
- [20] B. J. Wood *et al.*, "Navigation systems for ablation," *Journal of Vascular and Interventional Radiology*. 2010.
- [21] S. Patil, J. Burgner, R. J. Webster, and R. Alterovitz, "Needle steering in 3-D Via rapid replanning," *IEEE Trans. Robot.*, 2014.
- [22] N. Abolhassani, R. Patel, and M. Moallem, "Needle insertion into soft tissue: A survey," *Med. Eng. Phys.*, 2007.
- [23] S. P. DiMaio and S. E. Salcudean, "Needle Insertion Modeling and Simulation," *IEEE Trans. Robot. Autom.*, 2003.
- [24] R. Taschereau, J. Pouliot, J. Roy, and D. Tremblay, "Seed misplacement and stabilizing needles in transperineal permanent prostate implants," *Radiother. Oncol.*, 2000.
- [25] H. Gray, *Anatomy, descriptive and surgical*, vol. 1. Lea Bros., 1897.
- [26] R. Alterovitz, K. Y. Goldberg, J. Pouliot, and I. C. Hsu, "Sensorless motion planning for medical needle insertion in deformable tissues," *IEEE Trans. Inf. Technol. Biomed.*, 2009.
- [27] S. Y. Ko and F. Rodriguez Y Baena, "Toward a miniaturized needle steering system with path planning for obstacle avoidance," *IEEE Trans. Biomed. Eng.*, 2013.



- [28] D. C. Rucker *et al.*, “Sliding mode control of steerable needles,” *IEEE Trans. Robot.*, 2013.
- [29] F. O. Maria-Joseph and T. Podder, “Sliding Mode Control of a Shape Memory Alloy Actuated Active Flexible Needle,” *Robotica*, vol. 36, no. 8, pp. 1188–1205, 2018.
- [30] R. J. Webster, J. S. Kim, N. J. Cowan, G. S. Chirikjian, and A. M. Okamura, “Nonholonomic modeling of needle steering,” in *International Journal of Robotics Research*, 2006.
- [31] K. G. Yan, T. Podder, Y. Yu, T. I. Liu, C. W. S. Cheng, and W. S. Ng, “Flexible needle-tissue interaction modeling with depth-varying mean parameter: Preliminary study,” *IEEE Trans. Biomed. Eng.*, vol. 56, no. 2, pp. 255–262, 2009.
- [32] R. G. Stock, N. N. Stone, Y. C. Lo, N. Malhado, J. Kao, and J. K. DeWyngaert, “Postimplant dosimetry for (125)I prostate implants: definitions and factors affecting outcome.,” *Int. J. Radiat. Oncol. Biol. Phys.*, vol. 48, no. 3, pp. 899–906, Oct. 2000.
- [33] T. L. De Jong, N. J. van de Berg, L. Tas, A. Moelker, J. Dankelman, and J. J. van den Dobbelsteen, “Needle placement errors: Do we need steerable needles in interventional radiology?,” *Med. Devices Evid. Res.*, vol. 37, no. 3, pp. 259–265, 2017.
- [34] E. Matheson, R. Secoli, C. Burrows, A. Leibinger, and F. Rodriguez y Baena, “Cyclic motion control for programmable bevel-tip needles to reduce tissue deformation,” *J. Med. Robot. Res.*, vol. 4, no. 01, p. 1842001, 2019.
- [35] F. Yang, M. Babaiasl, and J. P. Swensen, “Fracture-directed steerable needles,” *J. Med. Robot. Res.*, vol. 4, no. 01, p. 1842002, 2019.
- [36] R. Tsumura, Y. Takishita, and H. Iwata, “Needle Insertion Control Method for Minimizing Both Deflection and Tissue Damage,” *J. Med. Robot. Res.*, vol. 4, no. 01, p. 1842005, 2019.

- [37] P. Moreira *et al.*, “The MIRIAM Robot: A Novel Robotic System for MR-Guided Needle Insertion in the Prostate,” *J. Med. Robot. Res.*, vol. 2, no. 4, p. 175006, 2017.
- [38] N. J. Cowan *et al.*, “Robotic needle steering: Design, modeling, planning, and image guidance,” in *Surgical Robotics*, 2011, pp. 557–582.
- [39] H. B. Gilbert, D. C. Rucker, and R. J. Webster, “Concentric tube robots: The state of the art and future directions,” *Springer Tracts Adv. Robot.*, vol. 114, pp. 253–269, 2016.
- [40] K. B. Reed *et al.*, “Robot-Assisted Needle Steering,” *IEEE Robot. Autom. Mag.*, vol. 18, no. 4, pp. 35–46, 2011.
- [41] T. R. Wedlick and A. M. Okamura, “Characterization of pre-curved needles for steering in tissue,” in *Annual International Conference of the IEEE Engineering in Medicine and Biology Society*, 2009, pp. 1200–1203.
- [42] S. Okazawa, R. Ebrahimi, J. Chuang, S. E. Salcudean, and R. Rohling, “Hand-held steerable needle device,” *IEEE/ASME Trans. Mechatronics*, vol. 10, no. 3, pp. 285–296, 2005.
- [43] P. J. Swaney, J. Burgner, H. B. Gilbert, and R. J. WebsterIII, “A flexure-based steerable needle: high curvature with reduced tissue damage,” *IEEE Trans. Biomed. Eng.*, vol. 60, no. 4, pp. 906–909, 2013.
- [44] R. J. Webster, J. M. Romano, S. Member, and N. J. Cowan, “Mechanics of Precurved-Tube Continuum Robots,” *Robot. IEEE Trans.*, vol. 25, no. 1, pp. 67–78, 2009.
- [45] P. Sears and P. Dupont, “A steerable needle technology using curved concentric tubes,” *IEEE Int. Conf. Intell. Robot. Syst.*, pp. 2850–2856, 2006.
- [46] N. Abolhassani, R. Patel, and M. Moallem, “Needle insertion into soft tissue: a

survey.,” *Med. Eng. Phys.*, vol. 29, no. 4, pp. 413–431, 2007.

- [47] S. Misra, K. B. Reed, B. W. Schafer, K. T. Ramesh, and A. Okamura, “Mechanics of flexible needles robotically steered through soft tissue.,” *Int. J. Rob. Res.*, vol. 29, no. 13, pp. 1640–1660, 2010.
- [48] T. K. Podder, A. P. Dicker, P. Hutapea, K. Darvish, and Y. Yu, “A novel curvilinear approach for prostate seed implantation,” *J. Med. Phys.*, vol. 39, no. 4, pp. 1887–1892, 2012.
- [49] B. Konh and T. K. Podder, “Design and Fabrication of a Robust Active Needle using SMA Wires,” *Des. Med. Devices Conf.*, 2017.
- [50] B. Padasdao and B. Konh, “Shape Memory Alloy Actuators in an Active Needle - Modeling , Precise Assembly, and Performance Evaluation,” *J. Manuf. Sci. Eng.*, vol. 143, no. 2, p. 021003 (10 pages), 2020.
- [51] B. Konh, D. Sasaki, T. K. Podder, and H. Ashrafiuon, “3D Manipulation of an Active Steerable Needle via Actuation of Multiple SMA Wires,” *Robotica*, p. 1–17 DOI 10.1017/S0263574719000705, 2019.
- [52] Z. Khashei Varnamkhasti and B. Konh, “Design and Performance Study of a Novel Minimally Invasive Active Surgical Needle,” *J. Med. Device.*, 2019.
- [53] Z. K. Varnamkhasti and B. Konh, “Compact 3D-Printed Active Flexible Needle for Percutaneous Procedures,” *Surg. Innov.*, vol. 27, no. 4, pp. 402–405, 2020.
- [54] “[https://www.activeneedle.com/.](https://www.activeneedle.com/)” .
- [55] D. C. Lagoudas, *Shape Memory Alloys: Modeling and Engineering Applications*. 2008.

- [56] K. Otsuka and X. Ren, “Physical metallurgy of Ti-Ni-based shape memory alloys,” *Progress in Materials Science*. 2005.
- [57] G. Rondelli, “Corrosion resistance tests on NiTi shape memory alloy,” *Biomaterials*, 1996.
- [58] J. Ryhänen *et al.*, “In vivo biocompatibility evaluation of nickel-titanium shape memory metal alloy: Muscle and perineural tissue responses and capsule membrane thickness,” *J. Biomed. Mater. Res.*, 1998.
- [59] I. Mihálcz, “Fundamental characteristics and design method for nickel-titanium shape memory alloy,” *Period. Polytech. Mech. Eng.*, 2001.
- [60] J. Mohd Jani, M. Leary, A. Subic, and M. A. Gibson, “A review of shape memory alloy research, applications and opportunities,” *Materials and Design*. 2014.
- [61] R. Pfeifer, C. W. Müller, C. Hurschler, S. Kaierle, V. Wesling, and H. Haferkamp, “Adaptable orthopedic shape memory implants,” in *Procedia CIRP*, 2013.
- [62] L. Torrisi, “The NiTi superelastic alloy application to the dentistry field,” *Biomed Mater Eng*, 1999.
- [63] A. Yamada *et al.*, “Preliminary design of the mechanical circulation assist device for Fontan circulation using shape memory alloy fibers,” in *IFMBE Proceedings*, 2013.
- [64] L. G. Machado and M. A. Savi, “Medical applications of shape memory alloys,” *Brazilian Journal of Medical and Biological Research*, vol. 36, no. 6. pp. 683–691, 2003.
- [65] N. Ma, G. Song, and H. J. Lee, “Position control of shape memory alloy actuators with internal electrical resistance feedback using neural networks,” *Smart Mater. Struct.*, 2004.

- [66] M. Carballo, Z. J. Pu, and K. H. Wu, "Variation of Electrical Resistance and the Elastic Modulus of Shape Memory Alloys under Different Loading and Temperature Conditions," *Journal of Intelligent Material Systems and Structures*, vol. 6, no. 4, pp. 557–565, 1995.
- [67] K. Mudgal and P. Ghorai, "A Review: Improvement in the Methods for Controlling of Shape Memory Alloy Actuator During the Last Decade," *Sens. Lett.*, 2015.
- [68] L. C. Brinson, "One-dimensional constitutive behavior of shape memory alloys: Thermomechanical derivation with non-constant material functions and redefined martensite internal variable," *J. Intell. Mater. Syst. Struct.*, vol. 4, no. 2, pp. 229–242, 1993.
- [69] J. L. Pons, *Emerging Actuator Technologies: A Micromechatronic Approach*. 2005.
- [70] Z. He, K. R. Gall, and L. C. Brinson, "Use of electrical resistance testing to redefine the transformation kinetics and phase diagram for shape-memory alloys," *Metall. Mater. Trans. A*, vol. 37, no. 3, pp. 579–587, 2006.
- [71] S. Karimi, B. Konh, and H. Ashrafiuon, "SMA Wire Characterization for 3D Steerable Active Devices," no. 40789. p. V001T07A003, 2018.
- [72] B. Konh, S. Karimi, and S. Miller, "Feasibility study of an active soft catheter actuated by SMA wires," in *Proceedings of SPIE - The International Society for Optical Engineering*, 2018, vol. 10602, pp. 1–5.
- [73] H. Sayyaadi, M. R. Zakerzadeh, and H. Salehi, "A comparative analysis of some one-dimensional shape memory alloy constitutive models based on experimental tests," *Sci. Iran.*, vol. 19, no. 2, pp. 249–257, 2012.
- [74] K. Tanaka, "Thermomechanical Sketch of Shape Memory Effect: One-Dimensional Tensile Behavior.," *Res Mech. Int. J. Struct. Mech. Mater. Sci.*, vol. 18, no. 3, pp. 251–263, 1986.

- [75] C. Liang and C. A. Rogers, "One-Dimensional Thermomechanical Constitutive Relations for Shape Memory Materials," *J. Intell. Mater. Syst. Struct.*, vol. 1, no. 2, pp. 207–234, 1990.
- [76] H. Prahlad and I. Chopra, "Comparative evaluation of shape memory alloy constitutive models with experimental data," *J. Intell. Mater. Syst. Struct.*, vol. 12, no. 6, pp. 383–395, 2001.
- [77] J. G. Boyd and D. C. Lagoudas, "A thermodynamical constitutive model for shape memory materials. Part I. The monolithic shape memory alloy," *Int. J. Plast.*, vol. 12, no. 6, pp. 805–842, 1996.
- [78] Y. Ivshin and T. J. Pence, "A Thermomechanical Model for a One Variant Shape Memory Material," *J. Intell. Mater. Syst. Struct.*, vol. 5, no. 4, pp. 455–473, 1994.
- [79] E. J. Graesser and F. A. Cozzarelli, "A Proposed Three-Dimensional Constitutive Model for Shape Memory Alloys," *J. Intell. Mater. Syst. Struct.*, vol. 5, no. 1, pp. 78–89, 1994.
- [80] M. Sreekumar, M. Singaperumal, T. Nagarajan, M. Zoppi, and R. Molfino, "Recent advances in nonlinear control technologies for shape memory alloy actuators," *J. Zhejiang Univ. A*, 2007.
- [81] L. C. Brinson, A. Bekker, and S. Hwang, "Deformation of shape memory alloys due to thermo-induced transformation," *J. Intell. Mater. Syst. Struct.*, 1996.
- [82] K. Ikuta, M. Tsukamoto, and S. Hirose, "Mathematical model and experimental verification of shape memory alloy for designing micro actuator," 2002.
- [83] A. S. Veeramani, G. D. Buckner, S. B. Owen, R. C. Cook, and G. Bolotin, "Modeling the dynamic behavior of a shape memory alloy actuated catheter," *Smart Mater. Struct.*, 2008.

- [84] G. V. Webb, D. C. Lagoudas, and A. J. Kurdila, "Hysteresis modeling of SMA actuators for control applications," *J. Intell. Mater. Syst. Struct.*, 1998.
- [85] K. Ikuta, M. Tsukamoto, and S. Hirose, "Shape memory alloy servo actuator system with electric resistance feedback and application for active endoscope," 2003.
- [86] K. Kuribayashi, "Improvement of the response of an SMA actuator using a temperature sensor," *Int. J. Rob. Res.*, 1991.
- [87] G. Song, B. Kelly, and B. N. Agrawal, "Active position control of a shape memory alloy wire actuated composite beam," *Smart Mater. Struct.*, 2000.
- [88] E. P. Da Silva, "Beam shape feedback control by means of a shape memory actuator," *Mater. Des.*, 2007.
- [89] J. Ko, M. B. Jun, G. Gilardi, E. Haslam, and E. J. Park, "Fuzzy PWM-PID control of cocontracting antagonistic shape memory alloy muscle pairs in an artificial finger," *Mechatronics*, 2011.
- [90] G. Song and N. Ma, "Control of shape memory alloy actuators using pulse-width pulse-frequency (PWPF) modulation," *J. Intell. Mater. Syst. Struct.*, 2003.
- [91] Kyu-Jin Cho, S. Au, and H. H. Asada, "Large-scale servo control using a matrix wire network for driving a large number of actuators," 2004.
- [92] Z. Shi, T. Wang, D. Liu, C. Ma, and X. Yuan, "A fuzzy PID-controlled SMA actuator for a two-DOF joint," *Chinese J. Aeronaut.*, 2014.
- [93] S. H. Liu, T. S. Huang, and J. Y. Yen, "Tracking control of shape-memory-alloy actuators based on self-sensing feedback and inverse hysteresis compensation," *Sensors*, 2010.

- [94] D. Grant and V. Hayward, "Variable Structure Control of Shape Memory Alloy Actuators," *IEEE Control Syst.*, 1997.
- [95] B. Selden, Kyu-Jin Cho, and H. H. Asada, "Segmented binary control of shape memory alloy actuator systems using the Peltier effect," 2004.
- [96] B. Selden, K. Cho, and H. H. Asada, "Segmented shape memory alloy actuators using hysteresis loop control," *Smart Mater. Struct.*, 2006.
- [97] H. J. Lee and J. J. Lee, "Time delay control of a shape memory alloy actuator," *Smart Mater. Struct.*, 2004.
- [98] S. B. Choi, Y. M. Han, J. H. Kim, and C. C. Cheong, "Force tracking control of a flexible gripper featuring shape memory alloy actuators," *Mechatronics*, 2001.
- [99] M. H. Elahinia, T. M. Seigler, D. J. Leo, and M. Ahmadian, "Nonlinear stress-based control of a rotary SMA-actuated manipulator," *J. Intell. Mater. Syst. Struct.*, 2004.
- [100] D. C. Lagoudas, *Shape memory alloys: modeling and engineering applications*, vol. 1. New York: Springer, 2008.
- [101] S. J. Furst and S. Seelecke, "Modeling and experimental characterization of the stress, strain, and resistance of shape memory alloy actuator wires with controlled power input," *J. Intell. Mater. Syst. Struct.*, 2012.



## List of Publications

### 1. SMA Wire Characterization for 3D Steerable Active Devices

S. Karimi, B. Konh, H. Ashrafiuon - 2018 Design of Medical Devices Conference, 2018.

In this work, the characteristics of multiple SMA-wire actuators actuated under tension loads while interacting to facilitate 3D steering in active steerable medical devices, were experimented. This study involved experimental measurements of the input electric current and electric potential difference across the SMA-wires, and calculation of the variations in electrical resistance of the SMA-wire actuators during actuation via *Ohm's law*. The achievable displacement profile by actuation (*Joule* heating) of the SMA-wire actuators, for a disc shaped geometry was obtained. This was used in subsequent studies on self-sensing actuators.

## **2. Feasibility study of an active soft catheter actuated by SMA wires**

B. Konh, S. Karimi, S. Miller – Proc. SPIE, Smart Structures and NDE for Industry 4.0, 2018.

Active catheters have the potential to revolutionize surgical procedures because of their computer-controlled and enhanced motion. This study assessed the feasibility of developing an active catheter using an arrangement of thin elastomer tubes and SMA-wire actuators. In this work, SMA wires were attached to thin pressurized elastomer tubes to realize deflection on the tubes. The tip motion achieved via actuation of SMA-wire actuator was measured and reported. The results of this study demonstrated the significance of training procedure in SMA-wire actuators on the required external loads for a consistent actuation of SMA-wire actuator

### **3. Towards the development of a triple SMA actuated vertical tube**

S. Karimi, B. Konh, E. Seidi – Proc. SPIE, Active and Passive Smart Structures and Integrated Systems XII, 2018.

In this work, an active vertically hung tube (the earliest prototype of the 3D steerable active flexible needle made of separate 3D-printed parts), was designed, fabricated, and tested. Three SMA-wire actuators were embedded on the exterior peripheral side of the tubes to realize a multi-directional motion, while pre-stressed by a mass attached to one end of the tube. The displacement profile of the active tube while actuated in two cases of absence and presence of an applied external load was captured and analyzed vision based. Variations in electrical resistance of the SMA-wire actuators were measured for further use in controlling the deflection of the tube in each direction. This work demonstrated the feasibility of creating a motion in 3D directions via actuation of three SMA-wire actuators distributed evenly on the tube design layout.

#### **4. 3D Steerable Active Surgical Needle**

S. Karimi, B. Konh – 2019 Design of Medical Devices Conference, 2019.

Minimally invasive needle-based surgical procedures for diagnostic and therapeutic purposes such as biopsy and brachytherapy demand precise navigation of the surgical needle in soft tissue. Active needle steering increases the target placement accuracy in percutaneous interventions, and consequently improves the clinical outcome. In this work, a novel 3D steerable SMA-activated surgical needle made of 3D printed rigid-link flexible-joint was proposed. The design provides an enhanced actuation capability by making use of multiple interacting SMA-wire actuators; offering a variety of actuation schemes to implement, enabling 3D motion of the needle at the tip. This work demonstrated the feasibility of 3D steerability through active control of multiple interacting SMA-wire actuators and introduced a promising approach in development of a 3D steerable active surgical needle with controllable 3D motion of the needle tip for minimally invasive surgical procedures.

**5. Self-Sensing Feedback Control of Multiple Interacting SMA Actuators in a 3D Steerable Active Needle – *accepted***

S. Karimi, B. Konh – Journal of Intelligent Material Systems and Structures, 2020.

In this work, the actuation response of the 3D steerable SMA-activated flexible needle in various actuation scenarios was analyzed to develop a kinematic model of the needle in actuation. The SMA-wire actuators were characterized in terms of their actuation strain, variations of electrical resistance during actuation, and the electric power required for actuation, to design a self-sensing electrical resistance feedback control system for reference tracking and position control of the active needle at the tip. The proposed control system was initially tested in position tracking control of a single SMA-wire actuator under applied stress to verify the performance of the designed control system in SMA control and was then implemented to control multiple interacting SMA-wire actuators and manipulate the 3D steerable active needle along a reference path. Results of this study introduced SMAs as promising alternatives for traditional actuators used in surgical instruments providing an enhanced design, full characterization advantages, and controllability.

## **6. Needle Tip Manipulation and Control of a 3D Steerable SMA-Activated Flexible Needle**

B. Konh, P. Berkelman, S. Karimi – 2020 IEEE RAS/EMBS International Conference on Biomedical Robotics and Biomechatronics, 2020.

In this study, the designed self-sensing resistive-based feedback loop control system was further developed, and the control parameters of the system were adjusted for precise actuation of the SMA-wire actuators. The control system relies on the electrical resistance measurement feedback to estimate the position of the needle tip during actuation duties of the SMA-wire actuators. The significance of SMA-wires as actuators in biomedical devices is the correlation between the actuation strain and variations in electrical resistance of the SMA-wire actuators, i.e., the actuation in SMA-wire actuators can be related to their electrical resistance. This allows a concomitant sensing and actuation (*smart actuation*) with SMAs. The control system is designed to accomplish a desired 3D motion of the needle tip, based on the concept of smart actuation. The accuracy and efficiency of the control algorithm in manipulating the 3D steerable active needle via precision control of the SMA-wire actuators was demonstrated.

## **7. Dynamic Characteristics Analysis and FEM Modeling of Flexible Joints of an SMA-activated Flexible Multi-Joint Needle**

S. Karimi, B. Konh – 2020 Design of Medical Devices Conference, 2020.

In this work, kinematics characteristics and dynamics analysis of the flexible multi-joint active surgical needle, with SMA-wire actuators were studied. Modelling the dynamics of the active needle in actuation is an essential step in predictions of the needle-tissue interactions, navigation, and control of the active needle, during insertion in the tissue. The study provides analysis on the dynamics of the active needle in actuation was analyzed to model the dynamics characteristics of the flexible joints for actuation control, and precise manipulation of the active needle. In kinematics modelling of the active needle, flexible joints are modeled as three independent compression/extension springs, rotating about the actuation axis of the corresponding SMA-wire actuators, i.e., axes of the three-axis coordinate systems.

# Appendix

## A1. Control Algorithm Flowchart

